IMMOBILIZED LAMININ 332 AND AMELOBLASTIN DERIVED PEPTIDES INCREASE KERATINOCYTE ADHESION ON TITANIUM SUBSTRATES.

A THESIS SUBMITTED TO THE FACULTY OF THE GRADUATE SCHOOL OF
THE UNIVERSITY OF MINNESOTA
BY

VASILIKI KOIDOU

IN PARTIAL FULFILMENT OF THE REQUIREMENTS
FOR THE DEGREE OF
MASTER OF SCIENCE

MAY 2017

AKNOWLEDGMENTS

I would like to acknowledge the continuous guidance and support of my advisor Dr Conrado Aparicio.

Dr James Hinrichs for opening the door of the Advanced Education Program in Periodontology at the University of Minnesota to me three years ago.

Dr Massimo Costalonga for his valuable directions and suggestions.

Dr Larry Wolff for serving on my examining committee, as well as for his continual support during the residency.

Dr Prokopis Argyris for his continual support during this project and for sharing his expertise with me.

Erik Skoe and Juliana Mota Siqueira for their important contributions on this work.

Dr Herzberg for allowing me to work on this project in his lab.

Dr Karen Ross for her help during this project.

Dr Lei Zhang for the data analysis.

Josette Fontana for her administrative support and facilitation.

DEDICATION

I would like to dedicate this Master Thesis to my family.

My father, Petros, who being devoted to Science himself, taught me early in life that goals can be achieved, that efforts eventually pay back and personal fulfilment comes through serving others. Being inspired by his persistence, I learned that one should pursue a career that he/she is passionate about.

My mother, Maria, who I admire indefinitely for the example she set forth for me and my sister and taught us that we need to respect first ourselves, before respecting others. Her endless support through good and bad times and the comfort she provides with the thought she will always be there.

My sister, Venetia, who is growing to become an amazing person and scientist. She has stood by me in the darkest times with understanding and affection. I miss her every day.

My grandparents, including the ones I lost during these three years, for their love and support.

George, for standing by me during the last six years with impeccable patience and kindness. For sharing this amazing journey with me.

Finally, to Greece and the Greek Public Educational system that provided me the necessary provisions to open my wings and set forth in this Endeavor.

"Excellence is never an accident. It is always the result of high intention, sincere effort, and intelligent execution; it represents the wise choice of many alternatives - choice, not chance, determines your destiny."
-Aristotle-

ABSTRACT

Background: Titanium (Ti) materials have been functionalized with biomolecules as a modern strategy to incorporate bioactive motifs to expand and improve their properties. Laminin 332 participates in the formation of hemidesmosomes, and promotes epithelial adhesion around teeth and implants. Ameloblastin, an enamel derived protein, is reportedly involved in the events following disruption of the periodontal ligament.
Objectives: To bio-functionalize Ti substrates with a Laminin 332 derived peptide (LAM), an Ameloblastin derived peptide (AMBN) or combinations of both peptides and assess keratinocyte adhesion on Ti substrates in each condition.
Methods: LAM, AMBN or combinations of both peptides were covalently immobilized on Ti discs. Successful immobilization of the peptides on Ti discs was confirmed by contact angle goniometry, XPS (X-ray photoelectron spectroscopy), and fluorescent labeling. Additionally, mechanical and thermochemical tests measuring the stability of the peptides on Ti substrates were performed. Immortalized oral keratinocytes (OKF6/TERT-2) were cultured on LAM, AMBN or combinations of both peptides Ti substrates. Hemidesmosome formation was investigated via immunofluorescence and western blot for 24 and 48 hours. Cell proliferation was also assessed at 1, 24 and 48h. Statistical analysis with linear regression models was utilized and the level of significance was set at 0.05.
Results: High amounts of well-anchored and homogeneously distributed peptides were identified on the Ti substrates. The immobilized peptides exhibited mechanical and thermochemical stability following *in vitro* simulated challenges. OKF-6/TERT-2 cell proliferation was increased in the LAM or AMBN coated discs at 48h of incubation, ($p<0.05$) The combinations of both peptides' coatings, however induced the highest hemidesmosome formation at 48h ($p<0.05$).
Conclusions: The immobilization of combination of LAM and AMBN derived peptides on Ti substrates promotes hemidesmosome formation at 48 hours. This finding is promising in the effort to establish a stable per-mucosal seal around dental implants.

This project was presented in the IADR General Session, March 2017, San Francisco, CA, USA under the title:

"IMMOBILIZED LAM AND AMBN INCREASE KERATINOCYTE ADHESION ON Ti SUBSTRATES. "
V.P. Koidou, P. P Argyris, E.P. Skoe, J. Mota Siqueira, X. Chen, J. Hinrichs, M. Costalonga, C. J. Aparicio.

Awarded the 2017 IADR Colgate Research in Prevention Award.

Awarded the Implantology Research Group, Young Investigator Award, for the Basic Research category.

TABLE OF CONTENTS

LIST OF TABLES

LIST OF FIGURES

BACKGROUND

1.1 Junctional Epithelium

Junctional epithelium (JE) is the component of the dento-gingival unit that rests in contact with the tooth surface (Figure 1). The innermost cells of the JE constitute a tight seal opposed to the mineralized tooth surface, the so called epithelial attachment *(Shroeder 1977)*. Junctional epithelium is formed during tooth eruption by the stratum intermedium of the reduced enamel epithelium and the oral epithelial cells *(Ten Cate 1998)*. However, this tissue may be replaced in time by junctional epithelium derived from the basal cells, originating from the oral gingival epithelium *(Ten Cate 1996)* or other epithelium *(Listgarten 1967)*.

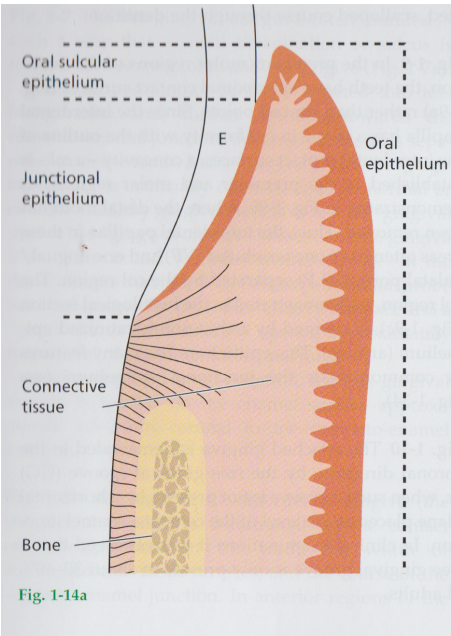

Figure 1. Localization of the junctional epithelium in the periodontal tissues. Adopted from: Lindhe et al. 2008.

The mediation of the junctional epithelium between the soft and mineralized periodontal tissues renders it important in tissue homeostasis, as well as in the defense against microorganisms and their products. The microorganisms, in close proximity to the junctional epithelium, are known to form complex ecological systems

that adhere to a glycoprotein layer called biofilm *(Schaudinn 2009)*. As a result of the formation of this biofilm, the neighboring periodontal tissues rest in a constant challenge. Lacking a keratinized layer, which would function as a physical barrier, like most epithelia do, other structural and functional mechanisms play the role of a protective barrier.

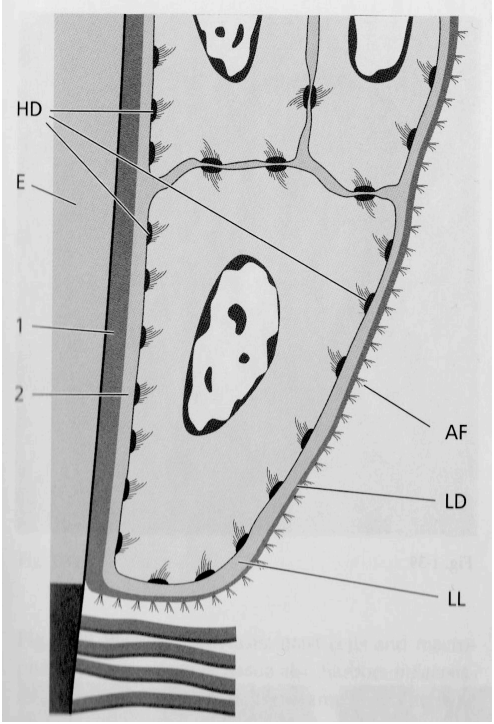

Figure 2. Microscopic anatomy of the junctional epithelium.
(HD:hemidesmosomes, E: enamel, LL/2: lamina lucida, LD/1: lamina densa)
Adopted from: Lindhe et al. 2008.

Junctional epithelium consists of 15 to 30 cell layers coronally and only 1 to 3 apically (Figure 2) *(Bosshardt 2005)*. It is stratified, non-keratinized epithelium made up of two strata: a basal layer and a supra basal layer. The basal layer cells face the connective tissue. The cell line of the supra basal layer that faces the tooth surface comprise the directly attached to the tooth cells or DAT cells *(Salonen 1989)* and these cells constitute the internal basal lamina (Figure 2). The internal basal lamina holds special characteristics and structure, in comparison to the external basal lamina that faces the connective tissue and resembles most other basement membranes. The internal basal lamina includes two layers: one electron lucent, the

lamina lucida and one electron dense, the lamina densa *(Schroeder 1977)* (Figure 2). Furthermore, the internal basal lamina lacks most basement membrane components such as collagen type IV and VII, most laminins, perlecan and a lamina fibroreticularis *(Salonen 1985, Kogaya 1989, Sawada 1990, Salonen 1991, Oyarzun-Droguett 1992; Hormia 2001)*. Interestingly however, laminin 332 is the only laminin isoform expressed in the internal basal lamina *(Oksonen 2001, Kinumatsu 2009, Hormia 1998, Mullen 1999).*

In natural dentition, the JE strongly attaches to cementum and enamel via the internal basal lamina (Figure 2) *(Salonen 1989)*. This attachment is considered to provide a biological seal against inflammation and is mediated by hemidesmosomes and focal contacts.

Laminin 332, as will be discussed in more detail, has been found to participate in the formation of those adhesion structures by interaction with integrins α6β4 and α3β1 *(Baker 1996, Hiroshaki 2000, Fuchs 1997)*. Integrin α3β1 is considered to be involved in the cell migration of the epithelial cells *(Fukushima 1998),* while integrin α6β4 has a critical role in cell adhesion through participation in the hemidesmosome formation *(Belkin 2000).*

The role of laminin 332 in the mediation of those adhesion structures is highly significant. Kinumatsu and colleagues showed a twelve-fold increase in the expression of laminin 332 in DAT cells, when compared to cells of the oral gingival epithelium, using immunofluorescence and quantitative real time PCR *(Kinumtsu 2009)*. In addition, the expression of α3β1 was four-fold higher in DAT cells, whereas that of integrin α6β4 was slightly higher for the DAT cells, compared to the oral

gingival epithelium. These data support the existence of a strong adherence system between the hard tissues and the junctional epithelium in teeth, where laminin 332 plays a highly significant role. The higher expression of integrin α3β1 concluded in this investigation, indicates that the DAT cells migrate on the enamel surface and their turnover is faster than the oral gingival epithelium. Sawada et al. most recently, used high resolution immunogold labeling in an animal model and reported that laminin 332 was present in the internal basal lamina and especially in the lamina densa, supporting that laminin 332 is a product of the junctional epithelium *(Sawada 2014, Sawada 2015)*.

1.2 Hemidesmosome

The hemidesmosome is a highly specialized integrin-mediated epithelial attachment structure (Figure 3) *(Walco 2015)*. While focal contacts have been attributed a more dynamic role, moving rapidly and assembling in the direction of migration of the epithelial cells, hemidesmosomes are considered to provide a more stable adhesion, assembling and moving just behind the focal contacts *(Ozawa 2010)*.

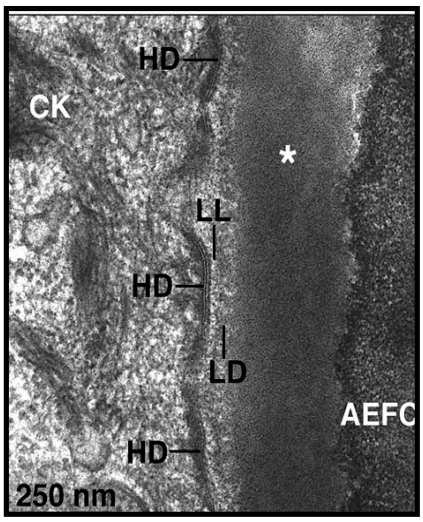

Figure 3. Transmission electron micrograph illustrating the internal basal lamina consisting of the lamina lucida (LL) and the lamina densa (LD) and hemidesmosomes (HD) at the interface between the junctional epithelium and the tooth. AEFC: acellular extrinsic fiber cementum, CK: cytokeratin filaments. Adopted from: Bosshardt et al. 2005.

Two types of hemidesmosomes can be observed, namely Type I and Type II that are differentiated based on their protein components *(Hieda 1992)*. Type I hemidesmosomes consist of five major components: namely integrin α6β4, plectin, tetraspanin CD151, bullus pemphigoid antigen 1 (BPAG1e or BP230) and bullus pemphigoid antigen 2 (BPAG2 or BP180 or type XVII collagen) (Figure 4)*(Owaribe 1990).* Type II hemidesmosomes consist of integrin α6β4 and plectin and lack the other antigens that participate in Type I hemidesmosomes.

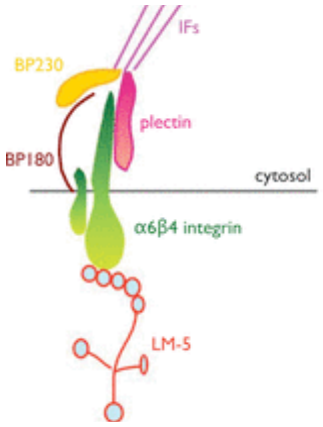

Figure 4. Type I Hemidesmosome composition. Adopted from: Streuli et al. 2009.

Inherited or acquired diseases that affect the hemidesmosome components are known to lead to a variety of skin blistering disorders, collectively known as epidermolysis bullosa (EB) that present with tissue separation and blister formation within different layers of the skin. Up to today, mutations in a minimum of twelve distinct genes encoding the components of the hemidesmosomes are considered responsible for the different types of epidermolysis bullosa *(Fine 2014).* Common clinical features of the condition include extreme skin fragility, blister formation and erosion in response to only minor mechanical trauma.

2.1 Laminin 332:

Laminins is a big family of conserved, multi domain, trimeric basement membrane proteins that consist of 3 chains: α, β and γ *(Aumailley 2005, Miner 2004)*. They participate in the formation of the extracellular matrix and play an important role for many cell functions such as adhesion, differentiation, migration, phenotype maintenance and resistance to apoptosis. Cell function is influenced by the induction of signaling pathways by laminins and via cell membrane receptors. Basement membranes are sheet-like extracellular matrix structures in close proximity to the cells. Laminins form networks with collagen type IV and affect the basement membrane related cells *(Yurchenco 2011).*

Up to today, 16 different isoforms of laminins have been identified in vertebrates *(Aumailley 2005)*. Although, laminins were previously named in Arabic numerals in the order they were discovered, they were recently renamed to a new identification system using three arabic numerals and based on the laminin's α, β, γ chain distribution *(Aumailley 2005)*. Laminin 5, as it was previously named, or laminin 332 precursor is secreted as a heterotrimer consisting of a 200-kDa α3 chain, a 140-kDa β3 chain and a 155-kDa γ2 chain, all of which are products of different genes *(Colognato 2000)*. In addition, the α3 and γ2 chains are processed to become a 165- and a 105-kDa polypeptide (Figure 5) *(Burgeson 1994)*. Laminin 332 is considered a primary expression and deposition of migrating keratinocytes, as shown in vivo by Zhang and Kramer *(Zhang 1996)*.

As a member of the laminin family, it has the ability to bind to certain molecules. Laminin 332 has shown the highest affinity for integrin α6β4 (*Nishiuchi 2006*) and is participating in the formation of adhesion structures, hemidesmosomes and focal

contacts, interacting with α6β4 and α3β1 integrins *(Baker 1996, Hirosaki 2000, Fuchs 1997)*.

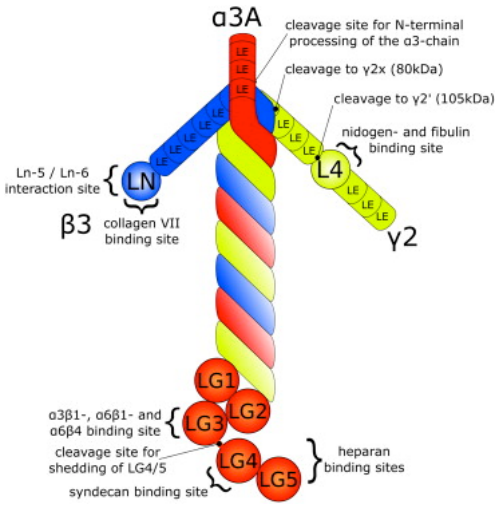

Figure 5. Molecular structure of Laminin 332. Adopted from: Schneider et al. 2007.

Besides laminin 332, the α3 chain is found in other laminins as well, whereas the β3 and γ2 chains are unique to laminin 332. The laminin α3 chain contains a C-terminal globular (LG) domain that consists of five globular modules LG1-LG5, each approximately 200 amino acid residues in length (Figure 5) *(Talts 1998, Timpl 2000).* Studies have mapped the adhesion site to integrins to the α3 chain. To date, the LG2 and LG3 globular modules have been recognized as specific binding sites for α3β1, while the LG4-LG5 fragment of the α3 chain does not possess any activity by itself *(Mizushima 1997, Tsubota 2000, Shang 2001)*. However, the binding site for integrin α6β4 has not yet been identified. This may be due to the fact that this site is cryptic and has to be released first by specific proteolytic processing of laminin 332, before interaction with α6β4 is possible. In contrast, recently a binding site of laminin 332 for both integrins was described *(Yamashita 2010).* CM6 is an antibody targeting the

1089 1094

sequence NERSVR of the rat α3 LG2 module of laminin 332. The particular antibody was found to disrupt the hemidesmosome formation induced by

the binding of laminin 332 with integrin α6β4. The effect of this antibody was additionally investigated on cell spreading, that is mediated by integrin α3β1 *(Fukushima 1998)*. The authors concluded that cell spreading was also significantly affected, thus suggesting that this antibody interacts with the binding sites of both integrins.

3.1 Peri-implant Junctional epithelium

Junctional epithelium around implants, or peri-implant junctional epithelium, is originating from the basal cells of the oral mucosa *(Fujii 1998).* Several investigators have attempted to answer the question of whether teeth and implant junctional epithelium possess similar structural and functional characteristics. It seems that the junctional epithelium both around teeth and titanium implants is structurally similar *(Berglundh 1991)*. In this context, Ikeda and colleagues suggested that the attachment of the internal basal lamina to the implant/titanium surface happens similarly as that found around a natural tooth, with the mediation of hemidesmosomes *(Ikeda 2000)*.

Interestingly though, hemidesmosomes have only been observed in the apical portion of the junctional epithelium around implants, while they are detected throughout the junctional epithelium in the tooth. Atsuta and co-investigators have linked the observation of the epithelial down-growth around implants with a diminished expression of laminin 332 in the junctional epithelium around a titanium implant. In particular, laminin 332 negative layers were observed for the coronal part of the peri-implant junctional epithelium, a positive layer of less than 50nm in the middle part of the epithelium, with no hemidesmosome formation and a layer of 100nm width in the most apical portion of the junctional epithelium, positive for hemidesmosomes (Figure 7)*(Atsuta 2005).*

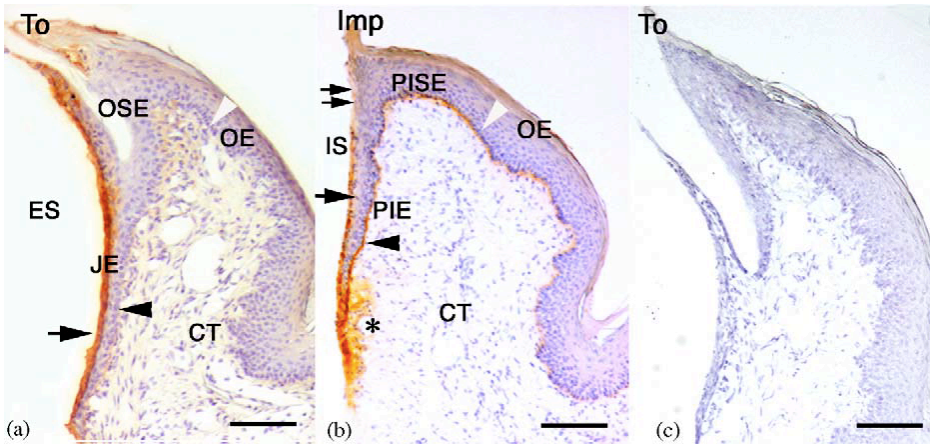

Figure 7. Light micrographs of the gingival around teeth (To) stained with anti-Ln-332 antibody (a) or with normal rabbit IgG (c) or oral mucosa around the titanium implant (Imp) with antibody (b). Adopted from: Atsuta et al. 2005.

4.1 Coatings for dental implants

Despite the high rates reported for implant survival and success, surface modification of titanium surfaces has gained significant attention in an attempt to expand the applications of dental implants, accelerate osseointegration and prevent peri-implantitis incidence, progression and subsequent implant loss.

Physical modifications of the titanium surfaces include the introduction of micro-roughness and nano-roughness though chemical etching, grit-blasting, plasma spraying or electrochemical processes of the surfaces, in order to achieve an improved micro-mechanical retention, as well as to positively reinforce the biological responses to the introduced surfaces *(Nazarpour 2014)*.

Furthermore, chemical modifications of dental implants by coating of implants with CaP is intended to release CaP into the peri-implant tissues, in order to increase the

saturation of body fluids and result in a biological apatite precipitation onto the surface of the implant that will serve as a matrix for osteogenesis. However, plasma-sprayed CaP coating has resulted in thick and rough coatings that lead to delamination of the coating from the surface and failure of the implant, due to the discrepancy in the dissolution behavior between the amorphous and crystalline CaP phases that make up the coating. By contrast, thin CaP coatings, such as the ones obtained by means of the PLD technology (pulsed laser beam resulting in a gaseous cloud), sputter coating, IBAD (ion beam-assisted deposition) and ESD (electrostatic spray deposition) are considered promising *(Junker 2009, Palmquist 2010).*

Finally, organic modifications of the titanium surfaces include two different approaches *(Nazarpour 2014)*: physisorbed coatings and covalently-bonded coatings. Physical absorption of organic molecules is achieved through immersion of the substrate in a solution of the bioactive molecule. A major drawback of this approach is the difficulty in controlling the density and the retention of the biomolecules on the surface that leads to the rapid loss of the bioactive properties. A modification of the psysisorption approach includes embedding of the biomolecules in a bioresorbable material utilized to coat the implant surface. Finally, a more promising approach includes immobilization of the molecules to the titanium substrate via covalent bonding and self-assembled mono-layers with silane or thiols coating. In contrast to the approach of physical absorption, the covalently bonded biomolecules are more stable and resistant to disruption during fabrication of the coating, as well as during the implantation of the material (*Schliephake 2008)*.

4.2 Previous approaches for tissue supply with laminin 332.

While the importance of the participation of laminin 332 in the adhesion structures of the junctional epithelium emerges, many efforts of supplying the peri-implant tissues with laminin 332 have been described in literature. The first step in this direction included immersion of the titanium alloy in solutions of the entire laminin 332 protein. The results of two such investigations concluded a notable increase in the hemidesmosome formation *(Tamura 1997, El-Grannam 1998)*. Furthermore, Ebihara and colleagues, in an in vitro model, highlighted the structural differences between the exogenous and endogenous laminin 332 regulation on human corneal epithelial cells (HCE). Interestingly the authors concluded that the addition of exogenous laminin 332 promoted corneal epithelial cell adhesion, spreading, as well as hemidesmosome formation, while the addition of endogenous laminin 332 presented a crucial role in cell migration *(Ebihara 2000)*. In this context, soluble laminin 332 was suggested by the authors as a potentially useful intervention for the treatment of recurrent corneal erosion.

Most recently, Werner et al. in 2009, used a laminin 332 derived peptide, as previously described by Kim and colleagues *(Kim 2005),* that will be described in more detail, employed on a multilayered polyelectrolyte film (MPF) on the titanium surface in order to promote keratinocyte attachment. The authors demonstrated a five-fold increase in hemidesmosome formation attributable to the attached peptide *(Werner 2009)*.

5.1 Laminin 332 derived peptide (LAM):

The 14-amino-acid peptide Pro-Pro-Phe-Leu-Met-Leu-Leu-Lys-Gly-Ser-Thr-Arg-Phe-Cys or PPFLMLLKGSTRFC is derived from the sequence of the LG3 globular domain of the laminin 332 α3 chain that was initially described by Kim and co-

workers *(Kim 2005)*. This sequence was found to be an active site for the binding of integrin α3β1 and implicated in cell adhesion and cell spreading of keratinocytes. The findings of the Kim et al. study agreed with previous investigations in that the LG3 domain of the α chain is crucial for the laminin 332 mediated activity *(Mizushima 1997, Tsubota 2000, Shang 2001).* The results of the investigation by Kim and co-workers thus suggested that the particular peptide of the LG3 domain is a novel motif capable of supporting α3β1-dependent cell adhesion and spreading.

Min and co-authors in 2010 utilized the peptide described by Kim and colleagues in an in vitro and in vivo study. Chitin microfibres were coated in vitro with the particular peptide and resulted in a statistically significant increase in cell attachment and cell spreading for both keratinocytes and fibroblasts. Chitin microfibers were coated with the same peptide in rat and rabbit full thickness cutaneous wounds and resulted in accelerated re-epithelialization, reduced inflammation (by means of reduced polymorphonuclear cell proliferation) and accelerated fibroblast proliferation. The results of the study thus highlighted the beneficial use of the sequence as a potential wound healing accelerator *(Min 2010)*.

Furthermore, Damodaran and colleagues in a rat model reported that the use of the laminin 332 derived peptide, incorporated in a Type I collagen scaffold, led to stimulated neurovascularization, decreased inflammatory cell infiltrate and accelerated wound healing *(Damodaran 2013)*. In addition, Oh and colleagues also supported the role of the above mentioned peptide in anti-apoptosis and promotion of cell growth of keratinocytes, thus promoting wound healing *(Oh 2009)*.

Finally, Werner et al. in 2009, incorporated this peptide *(Kim 2005)* in a multilayered polyelectrolite film on a titanium surface in vitro, and demonstrated both superior keratinocyte cell attachment and cell spreading, as well as a five-fold increase in the hemidesmosome formation at 24 hours after seeding. However, in an in vivo dog model, no histological differences were observed between laminin 332-derived peptide coated and non-coated implants, after 6 months of healing *(Werner 2009)*. Concluding, the authors highlighted the importance of investigations regarding cell kinetics at earlier time points and potential alternative methods to incorporate the peptides on the metallic substrate to enhance interactions in vivo.

6.1 Ameloblastin:

Ameloblastin, also known as sheathlin and amelin, is a member of the family of enamel matrix proteins and was for long time considered to be involved in the secretory stage of ameloblasts during tooth formation *(Lee 1996, Krebsbach 1996)*. However, quite recently it was shown to possess a role of signaling molecule and perform other functions as well. Ameloblastin has been found to be expressed by osteoblasts *(Spahr 2006)*, cementoblasts *(Nunez 2010)*, and epithelial rests of Malassez in the periodontal ligament *(Hasegawa 2003)*. In particular, Hasegawa and colleagues demonstrated that 7 days after mechanical injury, experimental root resorption was induced in a rat model. During root resorption, the epithelial rests of Malassez were found to express BMP-2; by contrast, during the early repair phases osteopontin and ameloblastin expression were upregulated.

Recently, ameloblastin has also been shown to mediate the adhesion of osteoblastic and fibroblastic cells on plastic or titanium surfaces *(Beyeler 2010)*. An active site promoting the adhesion activity of ameloblastin was identified by Beyeler in 2010 that

could be narrowed down to a sequence of 13 amino acid residues (VPIMDFADPQFPT).

In addition, the presence of ameloblastin has been reported in vitro to significantly enhance the attachment of mice periodontal cells at 1 and 4 hours, through RhoA and reduce their proliferation at 24 and 48 hours, through the kinase inhibitor p27 *(Zhang 2011)*. In contrast, another study, employing recombinant mouse ameloblastin, similar with amelogenin, was found to increase the periodontal cell attachment and proliferation in an in vitro model. Thus, ameloblastin was considered to possess a growth factor effect for the proliferation of periodontal ligament cells *(Zeichner-David 2006*).

Regarding epithelial cells, Saito and co-workers purified recombinant human ameloblastin, in an effort to assess the biological effect of the molecule in the epithelial cells. Using flow cytometric analysis, ameloblastin was found to inhibit the epithelial cell proliferation in vitro and arrest the G1 phase of the epithelial cell cycle. The authors suggested that ameloblastin may prevent the down growth of epithelium and thereby the initiation of periodontitis, through suppression of the epithelial cell proliferation (*Saito 2014)*.

Finally, in a rat model subjected to experimental orthodontic tooth movement and gingivectomy, ameloblastin was produced by Hertwig's epithelial root sheath (HERS) cells trapped in cementum five days after disruption of the periodontium *(Nishio 2010)*. These findings suggest that ameloblastin plays a role in the regeneration and healing after epithelial disruption. Furthermore, in a mouse model that does not express the full length ameloblastin, but rather a truncated form of it, Wazen et al. demonstrated not only presence of defects in the oral mineralized tissues, but also, and most interestingly, an interdental junctional epithelium that exhibited an irregular

outline with desquamating epithelial cells *(Wazen 2009).* These findings suggest that ameloblastin is implicated in events beyond enamel formation and can possibly imply that ameloblastin may hold a role in the formation, regeneration and healing after epithelial disruption, that have been minimally investigated to date.

6.2. Ameloblastin derived peptide (AMBN)

An active site in the protein ameloblastin was identified by Beyeler in 2010 *(Beyeler 2010)* that could be narrowed down to a sequence of 13 amino acid residues Val-Pro-Ile-Met-Asp-Phe-Ala-Asp-Pro-Gln-Phe-Pro-The or VPIMDFADPQFPT derived from exon 7 of the rat ameloblastin gene or exons 7–9 of the human gene, that have experienced a triplication of the active exon during evolution. This binding site seems to interact with cellular fibronectin, which in turn binds to integrin receptors. This sequence has been shown to promote cell adhesion of fibroblasts and osteoblasts on plastic or titanium surfaces and the authors suggested a possible benefit when the peptide will be used in dental applications such as coatings for dental implants.

7.1 Properties of LAM and AMBN peptides

The molecular properties of the selected peptides are shown in Table 1, namely the laminin 332 derived peptide (LAM) *(Kim 2005)* and the ameloblastin derived peptide (AMBN) *(Beyeler 2010)* are presented.

	Laminin 332 derived peptide (LAM)	Ameloblastin derived peptide (AMBN)
Single letter	PPFLMLLKGSTRFC	VPIMDFADPQFPT
Triple letter	Pro-Pro-Phe-Leu-Met-Leu-Leu-Lys-Gly-Ser-Thr-Arg-Phe-Cys	Val-Pro-Ile-Met-Asp-Phe-Ala-Asp-Pro-Gln-Phe-Pro-Thr
Hydrophobic/ Hydrophilic	60% hydrophobic - 40% hydrophilic	60% hydrophobic - 40% hydrophilic
Molecular Weight	1610.02g/mol	1477.7g/mol
Isoelectric Point	pH 10.55	pH 0.6
Net Charge at pH=7	2	-2

Table 1. Molecular properties of the LAM and AMBN peptide.

Objective

The objective of this study was to evaluate the effect of bio-functionalization of laminin 332 (LAM), ameloblastin (AMBN) derived peptides, or combinations of both on the keratinocyte cell proliferation and hemidesmosome formation on Ti substrates.

Working Hypotheses

1. Bio-functionalized Ti surfaces with laminin 332 (LAM) or ameloblastin derived peptide (AMBN) increase keratinocyte cell proliferation and hemidesmosome formation when compared to uncoated Ti surfaces.
2. Co-immobilization of laminin 332 (LAM) and ameloblastin derived peptides (AMBN) on Ti surfaces increases keratinocyte cell proliferation and hemidesmosome formation, when compared to the Ti surfaces coated with only laminin 332 derived peptides (LAM) and only with ameloblastin derived peptides (AMBN).

Specific Aims

The aims of the present study are:

1. To obtain stable coatings of biofunctionalized Ti substrates with the laminin derived peptide (LAM) or the ameloblastin derived peptide (AMBN) or combinations of both peptides.
2. To characterize the physical, chemical, and morphological properties of the immobilized Ti substrates by means of water contact angle goniometry, X-ray photoelectron spectroscopy (XPS), and visualization of fluorescently-labeled peptides, respectively.
3. To determine the mechanical and thermochemical stability of the peptide coatings on Ti substrates after in vitro challenges.
4. To assess cell proliferation and hemidesmosome formation of human keratinocytes on immobilized Ti substrates via Immunofluorescence and Western Blot.

Tested Groups

To test the working hypotheses and achieve the specific aims of this work, the following groups were studied (Table 2):

1. eTi: alkaline etched Ti discs, control
2. eTi-Sil: eTi + silanization treatment, control
3. GL13K: eTi-Sil with immobilized GL13K peptides (antimicrobial peptide), control
4. LAM: eTi-Sil with immobilized LAM peptides
5. AMBN: eTi-Sil with immobilized ABMN peptides
6. LAM+AMBN: eTi-Sil with sequential immobilization of LAM first and AMBN second peptides.
7. AMBN+LAM: eTi-Sil with sequential immobilization of AMBN first and LAM second peptides.
8. LAM/AMBN: eTi-Sil with simultaneous immobilization of LAM and AMBN peptides.

GROUP	DESCRIPTION
eTi	Alkaline etched Ti
eTi-Sil	Silanized Ti
GL13K	Immobilized GL13K
LAM	Immobilized LAM
AMBN	Immobilized AMBN
LAM+AMBN	Sequential immobilization LAM + AMBN
AMBN+LAM	Sequential immobilization AMBN + LAM
LAM/AMBN	Simultaneous immobilization LAM + AMBN

Table 2. Nomenclature of control and experimental groups.

MATERIAL AND METHODS

Peptides:

The 14-amino acid laminin 332 derived peptide (LAM) with sequence Pro-Pro-Phe-Leu-Met-Leu-Leu-Lys-Gly-Ser-Thr-Arg-Phe-Cys or PPFLMLLKGSTRFC is derived from the sequence of the LG3 globular domain of the laminin 332 α3 chain (*Kim 2005).* The second peptide utilized is the ameloblastin derived (AMBN) 13-amino acid peptide Val-Pro-Ile-Met-Asp-Phe-Ala-Asp-Pro-Gln-Phe-Pro-Thr or VPIMDFADPQFPT. This peptide is derived from exons 7 to 9 of the human AMBN gene *(Beyeler 2010)*. For the present investigation, and to favor the anchoring of the peptides on surfaces, we designed our peptides with two or three additional lysines (K) – each one provides with a potentially reacting free amine- at their N-terminus. Three Glycines (G) were used as the spacer between the lysines and the enzyme cleavable portion. Thus, the sequences utilized were: KKGGG-PPFLMLLKGSTRFC for LAM and KKKGGG-VPIMDFADPQFPT for AMBN.

Laminin 332 (LAM) and ameloblastin (AMBN) derived oligopeptides (purity >98%) as well as fluorescently-labelled oligopeptides, in particular Green fluorescence probe labeled AMBN (KKKGGG—VPIMDFADPQFPT-TK-5,6-FAM) and Red fluorescence probe labeled LAM (KKGGG-PPFLMLLKGSTRFC-K-5-TAMRA) were synthesized by solid-phase peptide synthesis (AAPPTec, Louisville, KY).

Titanium surface preparation:

Commercially pure Grade II Titanium discs (1mm thick, 6mm in diameter) (McMaster-Carr, Robbinsville, NJ) were punched from 10x10cm sheets, ground with papers with decreasing SiC-particle size, and finally polished with a suspension of alumina

particles (1.0_m and 0.5_m of mean size) on cotton clothes. The discs were cleaned by ultra-sonication in cyclohexane, isopropanol, ethanol (Sigma-Aldrich St.Louis, MO), deionized water (Mili-Q Plus) and acetone (Sigma-Aldrich St.Louis, MO) and dried with N_2 gas. Subsequently, the polished surfaces were activated by etching in 10ml of 5M NaOH (Sigma-Aldrich St.Louis, MO) overnight at 60 ^{o}C, then cleaned with deionized water for 30min and dried with N2 gas.

Silanization:

The protocol for silanization of the substrates has been described previously *(Chen 2013)*. Briefly, after activation, the samples were introduced in a N_2-saturated glass vessel and immersed for 1 h at room temperature in a pentane solution containing 0.05 M of N,N-diisopropylethylamine and 0.5 M of 3-chloropropyl-(triethoxy)silane (CPTES) (Sigma-Aldrich, St.Louis, MO). The 1 h immersion period consisted of 5 cycles of 10 minute rest and 2 minute sonication. Afterwards, the samples were ultra-sonicated successively in ethanol, isopropyl alcohol, deionized water and acetone, and dried with N_2 gas.

Immobilization of peptides:

For immobilization of the peptides, the silanized Ti discs were immersed in the 0.1 nM laminin 332 derived peptide (LAM) solution, 0.1 mM ameloblastin derived peptide (AMBN) solution or combinations of both peptides 0.1 mM solutions in 0.5mg/ml Na_2CO_3 overnight, in a desiccator in an atmosphere saturated with Ar and then rinsed with deionized water to produce the covalent conjugation of the peptides on the silanized titanium discs.

The experimental and control groups produced along with their corresponding nomenclature are presented in Table 2.

For the combination groups, including both the LAM and the AMBN peptides, the following sequences were produced and tested:

1) Silanized Ti discs were submerged in a solution of 0.1mM LAM for 24hrs, followed by submersion in 0.1mM AMBN peptide solution for 24hrs (LAM+AMBN group); 2) silanized Ti discs were submerged in 0.1mM AMBN solution for 24hrs, followed by immersion in 0.1mM LAM peptide solution for 24hrs (AMBN+LAM group); 3) silanized Ti discs were submerged in a solution of 1:1 mixed LAM and AMBN peptides and simultaneously co-immobilized with the two peptides overnight (LAM/AMBN group).

Surface Characterization:

X-ray photoelectron spectroscopy (XPS)

XPS was performed (SSX-100, Al Kα x-ray, 1mm spot size, 35° take-off angle) to characterize the atomic composition of the surfaces of the produced substrates. Survey scans (0-1100 binding energy, 8scans/sample) were done at 1eV step-size. The peak fittings and semi-quantification of the surface chemical composition were conducted using ESCA 2005 software provided with the XPS system.

Water Contact Angle Goniometry

Sessile drop contact angle measurements on the produced specimens were performed using a contact angle analyzer (DM-CE1, Kyowa Interface Science, Japan) with appropriate software (FAMAS, Kyowa Interface Science, Japan). Deionized water was used as the wetting liquid with a drop

volume of 2μL. Dynamic measurements consisted of capturing contact angles at a rate of 1 measurement per second for a time period of 50 seconds. The measurements were performed in triplicate.

Peptides' visualization by fluorescent labeling

Fluorescently labeled GL13K-TAMRA (green), LAM-FAM (red) and AMBN-TAMRA (green) was covalently immobilized on the Ti surfaces alone (GL13K, LAM only and AMBN only groups), or combined under the different co-immobilization conditions. Three samples were used for each group. After immobilization, samples were collected, rinsed with distilled water and acetone, and the fluorescence signals on surfaces were read with a synergy TM 2 multi-mode microplate reader (BioTek, Winooski, VT). AMBN or GL13K signal intensity was read as surface OD value at a wavelength of 485/528nm and LAM was read at 575/620 nm. Surface fluorescence intensities were also observed under multi-channel fluorescence microscope (Eclipse E800, Nikon, Japan).

Mechanical and Thermochemical Stability of the Coatings

The various peptide coatings produced were mechanically challenged by ultrasonication in deionized water for 2h. Following the mechanical challenge, the samples were characterized with XPS and water contact angle goniometry. In addition to the mechanical stability challenges, the samples were exposed to a thermochemical challenge via submersion in phosphate buffer solution (PBS, pH 7.4, 37°C) for 5 and 8 days followed by surface characterization via XPS and water contact angle goniometry.

In vitro Cell Experiments:

Keratinocyte culture

The cells used for the *in vitro* experiments are derived from a non-tumoral, immortalized oral keratinocyte cell line, OKF-6/TERT-2 (BWH Cell Culture and Microscopy Core, Boston, MA, USA). The cells were cultivated at 37^{o}C, in a sterile atmosphere of 5% CO2, in defined keratinocyte serum-free medium [K-SFM(1X)] (Thermo Fischer Scientific, Waltham, MA, USA) supplemented with a cocktail of growth factors including Epidermal Growth Factor (EGF) and Bovine Pituitary Extract (BPE) that allow cell growth under serum-free conditions (Thermo Fischer Scientific, Waltham, MA, USA). The medium was changed every two days. OKF-6/TERT-2 cells after passage four were utilized for all experiments.

Assessment of Hemidesmosome formation by Immunofluorescence Microscopy

One x 10^{5} OKF-6/TERT-2 cells were allowed to attach to the various Ti substrates for 24 or 48 hours, then were rinsed with PBS and fixed in ice cold methanol for 15 minutes, at room temperature. Cells were then rinsed twice with ice cold PBS for 5 minutes each and were incubated in 1% BSA in PBST for 30 minutes to block the non-specific binding of the primary antibody. The hemidesmosomes were detected with the use of a primary rabbit polyclonal antibody that specifically targets human collagen XVII (BP180), ab28440 (Abcam, Cambridge, MA, USA). The primary antibody was diluted in 1% BSA in PBST at 1:350 and the cells were incubated for 1 hour in a humidified chamber, followed by three washes of PBS, 5 minutes each. The cells were incubated for 60 minutes in an Alexa Fluor 488-conjugated goat anti-rabbit IgG (H+L) secondary antibody (#A-11034, Thermo Fischer Scientific, Waltham, MA, USA) in 1% BSA in PBST (1:500 dilution). Finally, cells were incubated for 5 minutes

in DAPI (4',6-Diamidino-2-Phenylindole, Dihydrochloride, D9542, Sigma-Aldrich, St. Louis, MO, USA) to stain the nucleic acids and thus, cell nuclei. The samples were mounted on slides using ProLong Gold Antifade mountant with DAPI (P36941, Thermo Fischer Scientific, Waltham, MA, USA) and covered with glass coverslips. Specimens were visualized with an upright fluorescence Nikon Eclipse E800 microscope via SPOT advance software (Spot Imaging, Sterling Heights, MI, USA). Images were subsequently analyzed and processed via ImageJ (ImageJ 1.49v, NIH, USA) under constant gamma, brightness and time exposure.

Immunofluorescence controls

Appropriate controls were performed including: controlling for background immunostaining reactivity in the absence of cells on the substrates and controlling for non-specific binding of the primary antibody, utilizing appropriate IgG isotope control in the same concentration as used for the main investigation.

Cell proliferation assay

Keratinocyte cell proliferation was assessed at 1, 24 or 48 hours of cell incubation on the various Ti substrates, via quantification of the number of DAPI-positive nuclei, stained as described above. Analysis was performed via Image J under constant gamma, brightness and time exposure.

Western Blot analysis

To further investigate the induction of hemidesmosome formation, Western Blot analysis of whole cell lysates for the various substrates at 48 hours was performed. Cells were washed twice with 1–2 ml ice-cold (4 °C) Dulbecco's-PBS and lysed in standard radioimmunoprecipitation assay (RIPA) buffer (Thermo Fischer Scientific,

Waltham, MA, USA). After centrifugation, soluble protein concentrations were measured using Bicinchoninic Acid (BCA) assay. Total protein (30 µl) was resolved using SDS-PAGE and transferred onto nitrocellulose membranes (Bio-Rad, Hercules, CA, USA). After transfer, the membrane was wet in PBS several times and subsequently blocked in Odyssey Blocking Buffer (Li-Cor, Lincoln, NE, USA) diluted 1:1 in PBS without Tween-20 for 1 hour in room temperature. Primary rabbit polyclonal anti-collagen XVII antibody (ab28440, Abcam, Cambridge, MA, USA) was diluted at 1:500 in Odyssey Blocking Buffer with 0.1% Tween-20, while 1:500 mouse anti-β-actin (sc-47778, Santa Cruz Biotechnology, Dallas, TX, USA) was used as a control. The blot was incubated in primary antibody solution at 4 ^{O}C overnight. The membrane was washed 4 times, for 5 minutes each, in room temperature in PBS with 0.1% Tween-20 with gently shaking. Then the membrane was incubated for 1 hour in Li-cor IRDye 800CW goat anti-rabbit (926-32211) and IRDye 680RD goat anti-mouse (926-68070) secondary antibodies, diluted at 1:5000 in Odyssey Blocking Buffer with Tween-20 (Li-Cor, Lincoln, NE, USA). Following the secondary antibody incubation, the membrane was washed 4 times, for 5 minutes each, at room temperature in PBS with 0.1% Tween-20 protected from light, rinsed with PBS to remove the residual Tween-20, and was scanned in the appropriate channels of a Li-cor Odyssey machine.

Statistical analysis

All the experiments were performed at least in triplicate. Results are summarized as average ± SD. For the variables, cell proliferation and hemidesmosome formation, one-way ANOVA was utilized for the between group comparisons and the comparisons over time. In order to adjust for multiple comparisons, the Bonferroni's method was used, e.g. if there were 5 comparisons for cell proliferation, p-value cutoff for statistical significance was set at 0.05/5=0.01.

RESULTS

Contact angle goniometry:

Figure 7 presents the contact angle goniometry results before and after the mechanical and thermochemical challenges. eTi displayed high hydrophilicity with low contact angles. After silanization, the surfaces became more hydrophobic, demonstrating higher contact angles. After immobilization of LAM, AMBN or combinations of both peptides, coated surfaces presented contact angle values that were either similar to the silanized substrates (LAM, LAM+AMBN, LAM/AMBN) or significantly lower than the silanized substrates (AMBN, AMBN+LAM). The control GL13K coated substrates showed significantly higher water contact angles when compared to the silanized or the rest of the immobilized substrates. Following the mechanical stability challenge, the substrates in eTi, LAM, LAM/AMBN and GL13K groups showed stable contact angles, whereas the eTi-Sil, AMBN, LAM+AMBN and AMBN+LAM groups experienced significant changes in contact angles. All groups except for GL13K and LAM+AMBN experienced further significant changes in water contact angle after thermochemical challenges.

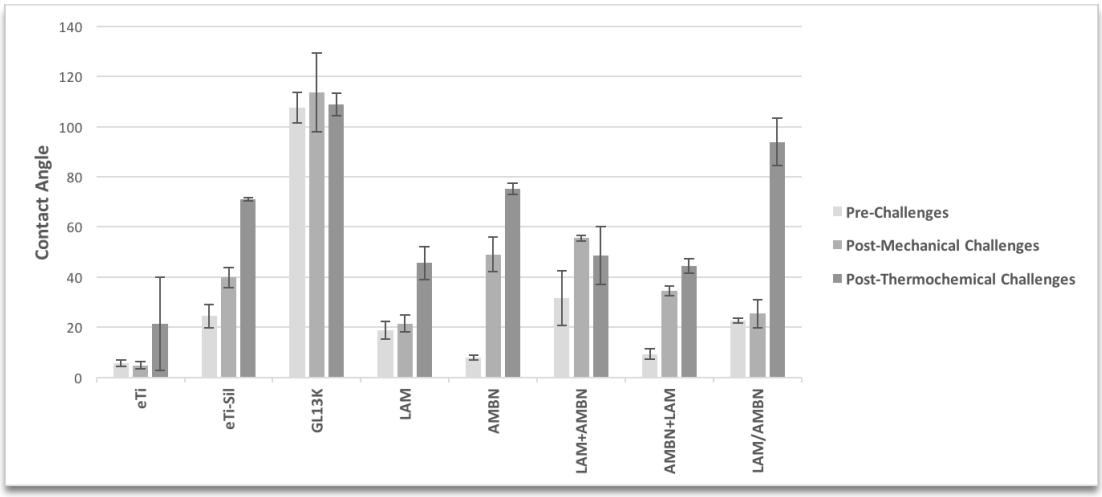

Figure 7. Contact angles before and after mechanical and thermochemical stability challenges.

XPS (X-ray photoelectron spectroscopy):

Figures 8, 9, 10 and Table 3 present the results of the XPS analysis before and after the mechanical and thermochemical challenges. The peaks present at 1071eV, 531eV, 460eV, and 290eV correspond to the signal of sodium, oxygen, titanium, and carbon, which dominate in the eTi and the eTi-Sil spectral signals. Due to the presence of amino groups in the LAM and AMBN and combination groups, the atomic percentages of both carbon and nitrogen (peak at 398eV) increased significantly following the application of the peptide coatings in all peptide-coated groups. Following the mechanical challenges, all groups with peptide coatings, except for the control GL13K, showed a notable decrease in the relative N percentage, but presented higher values than the control eTi and eTi-Sil substrates. Regarding the N/Ti ratio, all groups presented stable values except for the LAM and the combination groups (LAM+AMBN, AMBN+LAM, LAM/AMBN) that presented a decrease. After the thermochemical challenges, all peptide coated surfaces presented a slightly increased N percentage, except for AMBN, and a notable decrease in the C percentage, with respect to the values after mechanical challenge. Finally, for all peptide coated groups, the N/Ti ratio decreased, except for the AMBN+LAM and control GL13K coated samples.

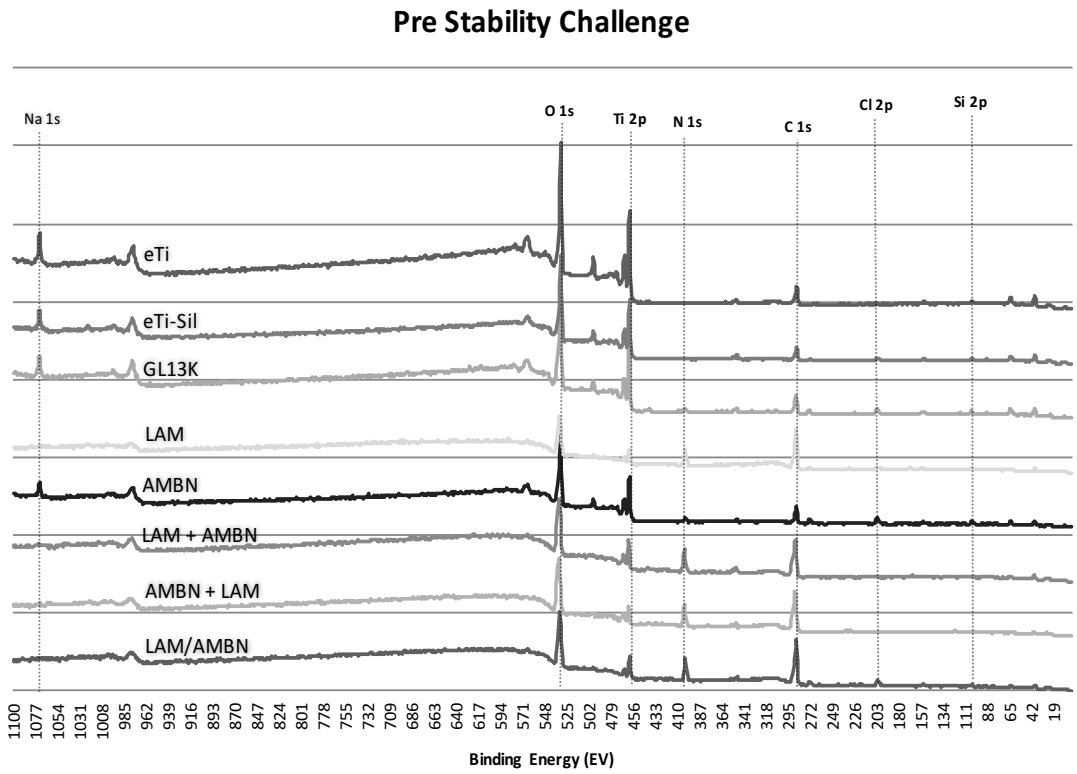

Figure 8. XPS analysis before challenges.

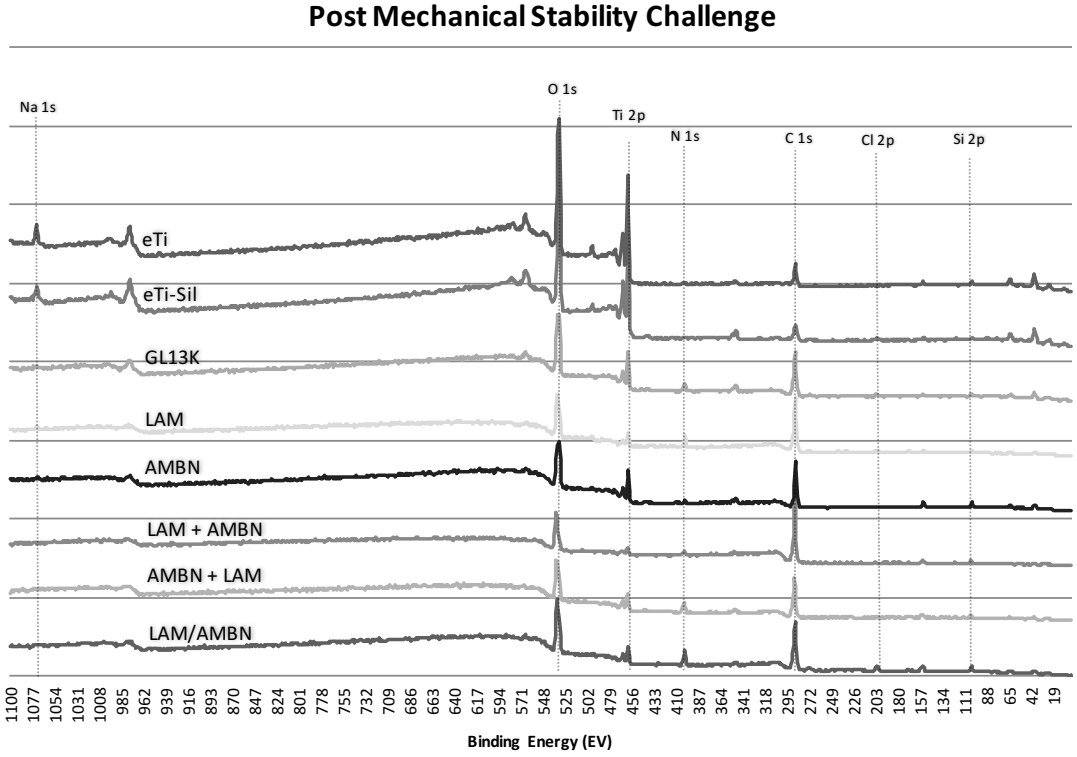

Figure 9. XPS analysis after mechanical challenges.

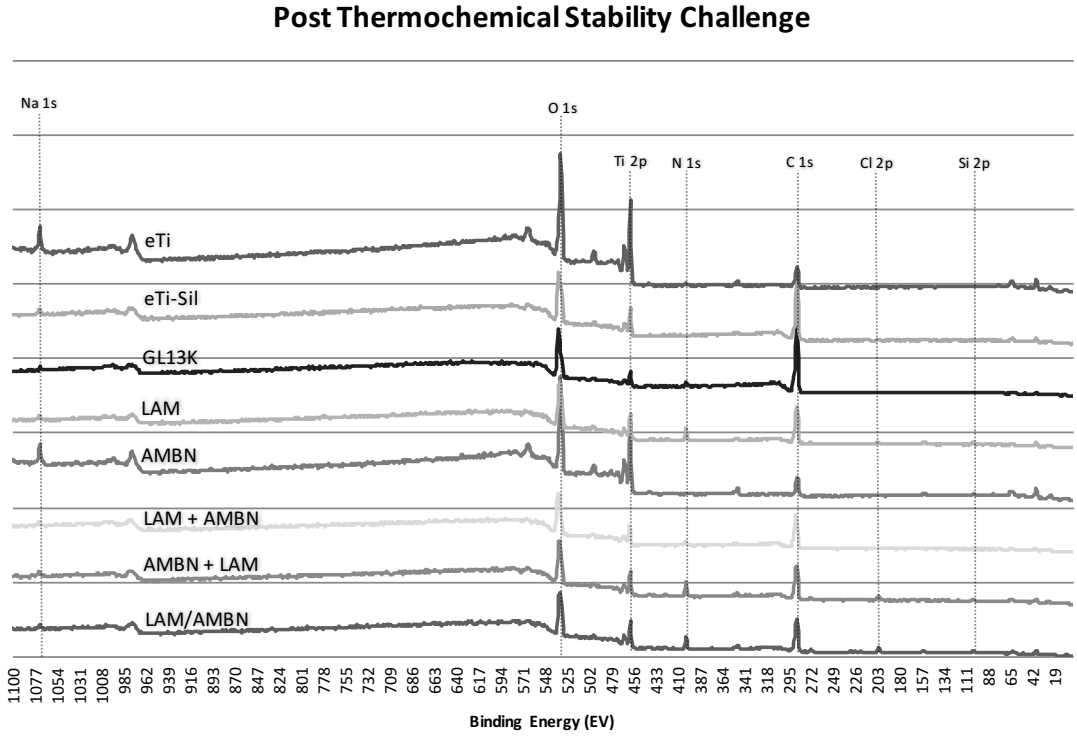

Figure 10. XPS analysis after thermochemical challenges.

		C1s	N1s	O1s	Si2p	Cl2p	Ti2p	Na1s	N/Ti	C/Ti
Pre Challenges	eTi	15.42 (8.07)	0.49 (0.02)	53.54 (4.81)	1.79 (2.21)	0.06 (0.16)	17.01 (2.59)	11.70 (2.73)	0.03	0.95
	eTi-Sil	15.51 (11.40)	0.50 (0.01)	47.05 (3.83)	1.83 (1.58)	1.27 (0.09)	23.27 (13.51)	10.56 (3.22)	0.03	0.97
	GL13K	38.13 (16.67)	5.57 (3.98)	38.05 (11.73)	2.46 (0.04)	2.22 (0.92)	8.62 (4.70)	4.95 (3.35)	0.91	5.82
	LAM	55.36 (2.52)	12.01 (1.55)	24.09 (0.26)	2.08 (0.30)	1.97 (0.74)	2.68 (0.18)	1.81 (0.15)	4.51	20.65
	AMBN	24.41 (6.22)	2.68 (0.42)	48.72 (7.48)	2.13 (2.32)	2.44 (2.46)	11.86 (1.16)	7.75 (1.93)	0.23	2.09
	LAM+AMBN	51.56 (0.11)	12.64 (1.04)	31.03 (1.21)	0.50 (0.68)	0.28 (0.23)	3.32 (0.42)	0.66 (0.04)	3.86	15.64
	AMBN+LAM	52.61 (2.79)	11.77 (2.81)	30.48 (4.17)	0.41 (0.10)	0.45 (0.21)	3.52 (2.14)	0.77 (0.40)	4.41	18.67
	LAM/AMBN	53.95 (1.45)	10.84 (0.11)	26.15 (2.10)	2.87 (1.33)	3.45 (0.70)	2.49 (1.06)	0.25 (0.43)	4.79	23.90
Post Mechanical Challenges	eTi	21.94	0.89	51.45	2.916	0	15.98	6.82	0.06	1.37
	eTi-Sil	19.77	0.65	56.39	0.96	0.85	16.66	4.72	0.04	1.19
	GL13K	49.40	5.22	33.06	3.82	1.32	6.20	0.97	0.84	7.97
	LAM	62.19	7.02	24.80	1.90	0.79	2.27	1.05	3.09	27.38
	AMBN	54.06	1.16	31.97	6.19	0.08	5.33	1.22	0.22	10.14
	LAM+AMBN	72.03	2.46	20.97	2.68	0.63	0.99	0.25	2.49	72.90
	AMBN+LAM	56.40	6.90	28.42	2.79	0.47	4.00	1.02	1.73	14.11
	LAM/AMBN	53.76	6.96	26.83	5.89	2.11	2.91	1.55	2.39	18.49
Post Chemical Challenges	eTi	24.85	0.77	52.21	0	0	14.18	7.99	0.05	1.75
	eTi-Sil	60.13	0.83	31.49	1.91	0.20	4.02	1.43	0.21	14.97
	GL13K	66.04	2.39	27.94	0.00	0.45	2.16	1.04	1.11	30.64
	LAM	50.12	8.18	29.96	3.87	1.51	4.61	1.75	1.77	10.87
	AMBN	25.29	1.16	49.40	3.26	0.58	12.95	7.36	0.09	1.95
	LAM+AMBN	53.14	3.25	35.95	1.13	0.30	4.11	2.12	0.79	12.94
	AMBN+LAM	48.22	8.82	29.83	2.83	2.12	4.87	3.31	1.81	9.91
	LAM/AMBN	45.89	7.79	32.67	3.04	3.24	5.27	2.09	1.48	8.70

Table 3. Atomic percentages observed for each atom before stability challenges, after mechanical challenge, and after thermochemical challenge. Numbers in brackets indicate standard deviation.

Fluorescence microscopy labeling:

As a qualitative study, the peptides immobilized on the substrates were visualized under fluorescent microscopy, after labelling with a Green fluorescence probe (GL13K-FAM or AMBN-FAM) and a Red fluorescence probe (LAM-TAMRA) (Figure 11). Untreated eTi and eTi-Sil uncoated surfaces were used as control and displayed no fluorescence signal. In contrast, fluorescence signal was observed for all peptide coated surfaces. GL13K and AMBN presented with significant green signal and no red signal. By contrast, LAM presented with significant red signal and no green signal. The three combination groups (LAM+AMBN, AMBN+LAM, LAM/AMBN) presented with less intense green and red signal, when compared to the monopeptide coatings, namely LAM or AMBN. In the merged channel, the combination groups (LAM+AMBN, AMBN+LAM, LAM/AMBN) presented with orange signal. After the mechanical and thermochemical challenges, the signals for all peptide coated groups were not significantly altered.

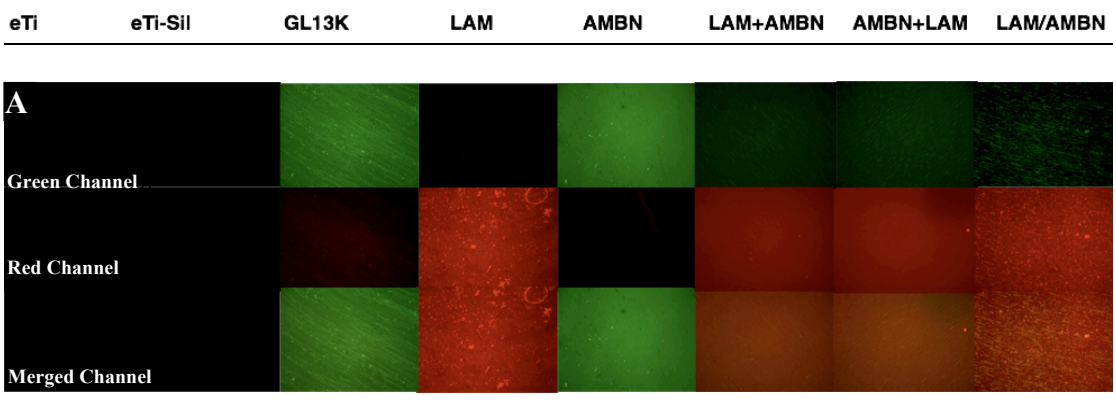

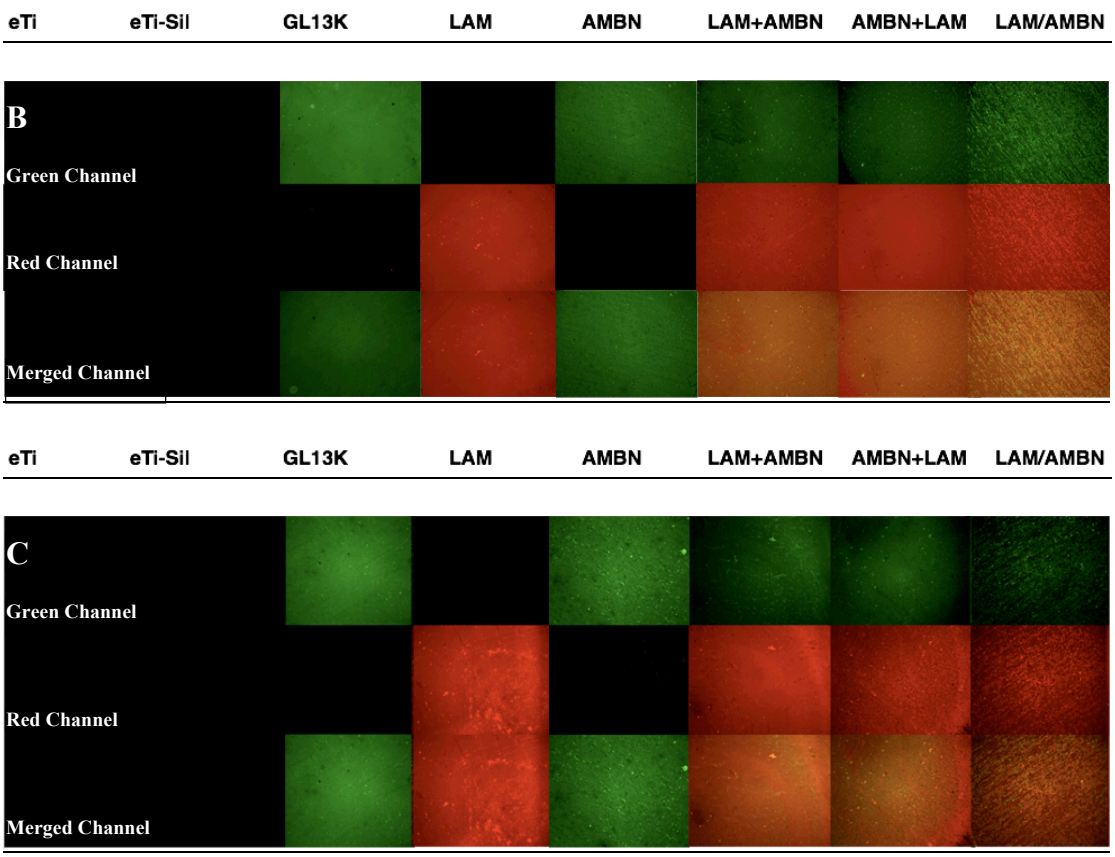

Figure 11. Visualization of fluorescently labelled peptides for all groups. A. before challenges, B. after mechanical challenges, C. after thermochemical challenges.

Cell proliferation:

OKF-6/TERT-2 cell proliferation was assessed on the different substrates after 1, 24 and 48 hours in culture. At 1h, the LAM group and the LAM and AMBN combinations (LAM+AMBN, AMBN+LAM, LAM/AMBN) enhanced the keratinocyte proliferation, when compared to the control substrates (eTi, eTi-Sil and GL13K) (Figure 12). At 24h, the LAM, AMBN, LAM+AMBN and AMBN+LAM substrates demonstrated superior number of cells on the substrates, when compared with the control substrates and this observed difference was statistically significant ($p<0.01$) (Figure 13). At 48h, The LAM and AMBN-coated surfaces enhanced keratinocyte proliferation, in comparison to the control Ti substrates (eTi, eTi-Sil, GL13K), with a higher number of cells at this time point ($p<0.01$) (Figure 14). Finally, over time all groups, except for LAM+AMBN, increased cell numbers on the substrates, suggesting that the treatments performed did not inhibit cell proliferation. (Figure 15) The group LAM+AMBN showed increased cell numbers from 1h to 24h. However, no further increase was noted from 24 to 48h.

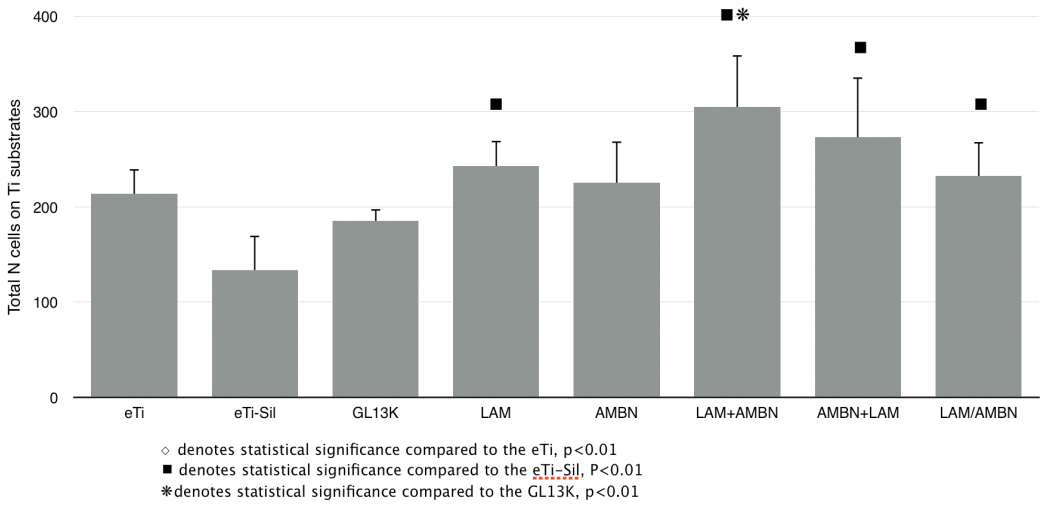

Figure 12. Cell proliferation for the substrates at 1h.

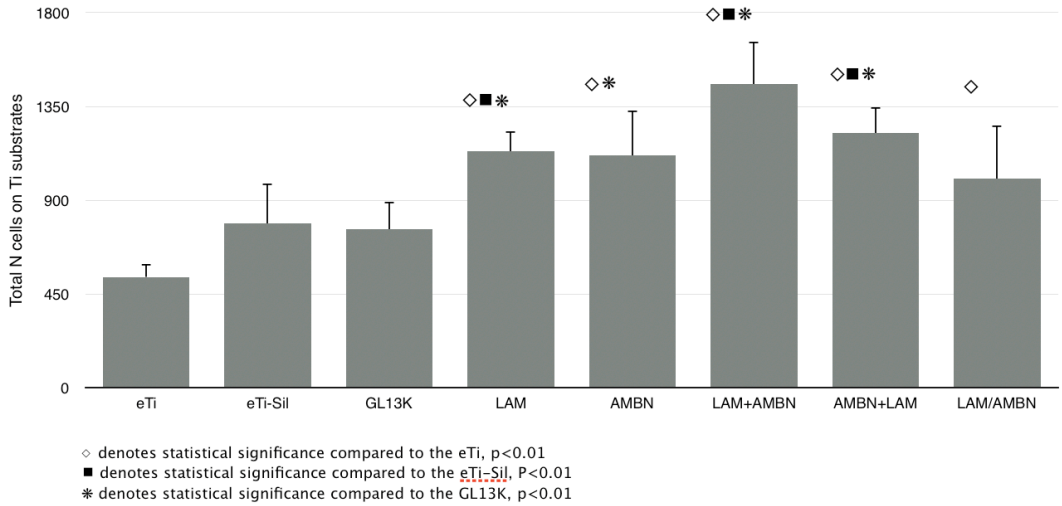

Figure 13. Cell proliferation for the substrates at 24h.

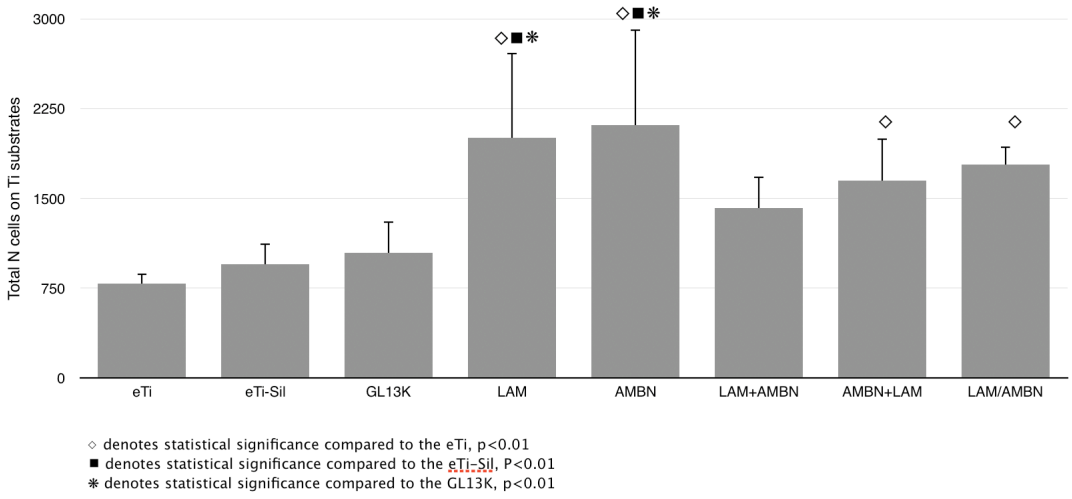

Figure 14. Cell proliferation for the substrates at 48h.

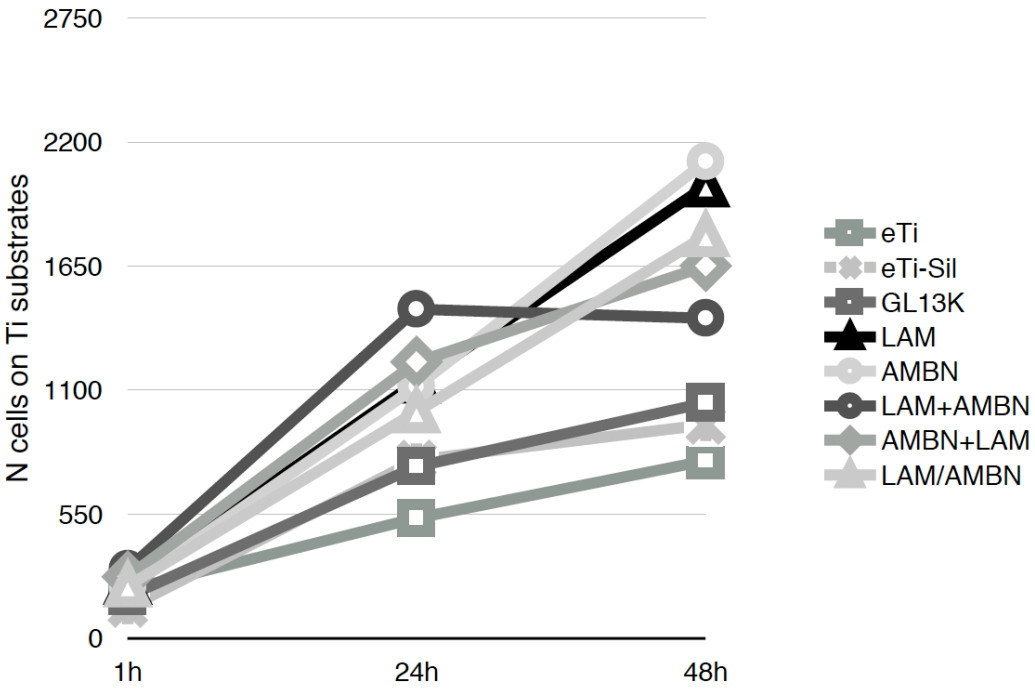

Figure 15. Cell proliferation for the substrates over time.

Hemidesmosome formation:

Hemidesmosome formation was assessed on the various substrates after 24 and 48h in culture via quantification of the intensity of the immunofluorescent staining for collagen XVII (BP180) and adjusting for background staining. IgG isotope control experiments were performed, in selected groups, and suggested that the non-specific binding of the primary antibody accounted for approximately 20% of the recorded fluorescence signal. At 24h, the LAM group and the co-immobilization groups, namely LAM+AMBN, AMBN+LAM and LAM/AMBN presented with statistically significant higher formation of hemidesmosomes, when compared to either of the controls: eTi, eTi-Sil or GL13K ($p<0.01$) (Figure 16). This significant difference remained after adjustment for the number of cells on the examined substrates. At 48h, the LAM, AMBN and the co-immobilization groups, namely LAM+AMBN,

AMBN+LAM and LAM/AMBN had statistically significant ($p<0.01$) higher formation of hemidesmosomes, when compared to either of the control groups: eTi, eTi-Sil or GL13K (Figure 17). In addition, the co-immobilization group AMBN+LAM presented with significantly higher hemidesmosome formation, when compared to the mono-peptide substrates (LAM or AMBN) ($p<0.005$). However, no significant differences were detected between the three co-immobilization groups ($p>0.005$). Over time, all groups presented with increasing hemidesmosome formation that was statistically significant different from 24 to 48h for the groups: LAM, LAM+AMBN, AMBN+LAM, LAM/AMBN ($p<0.05$) (Figure 18).

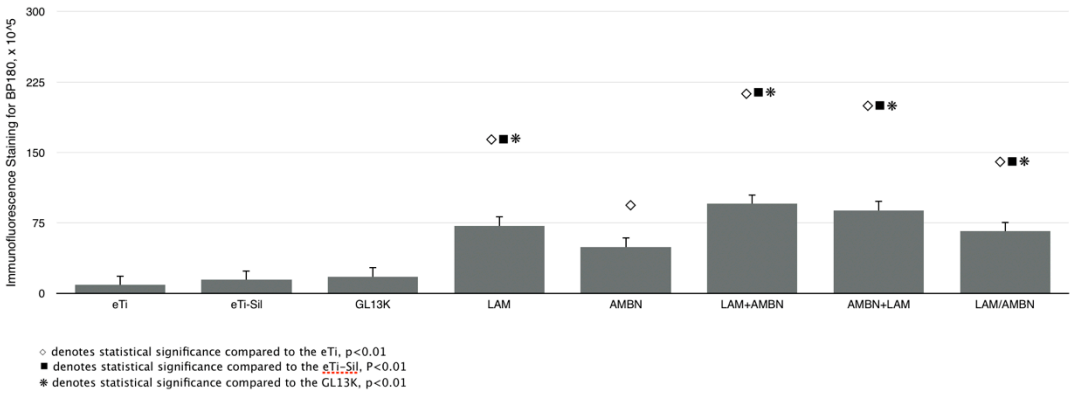

Figure 16. Hemidesmosome formation for the substrates at 24h.

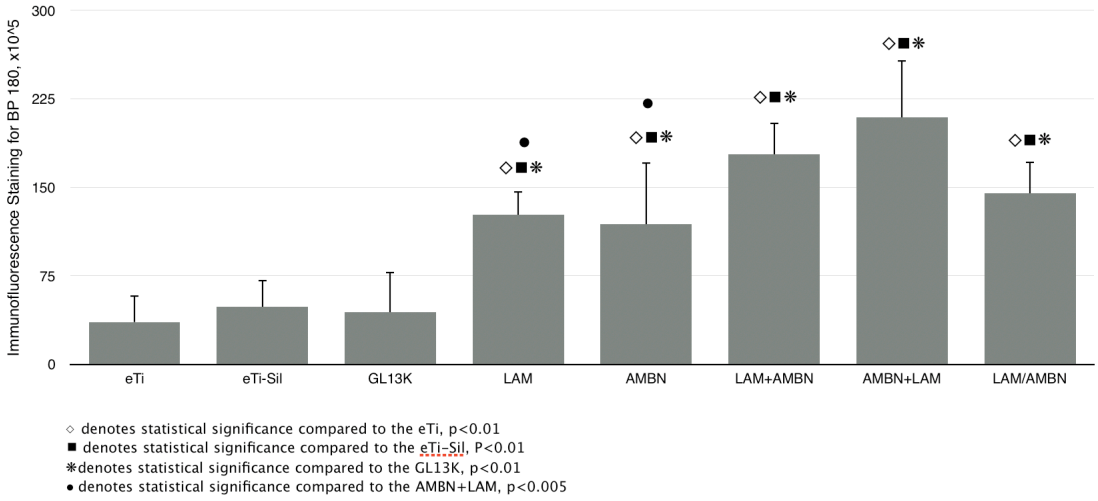

Figure 17. Hemidesmosome formation for the substrates at 48h.

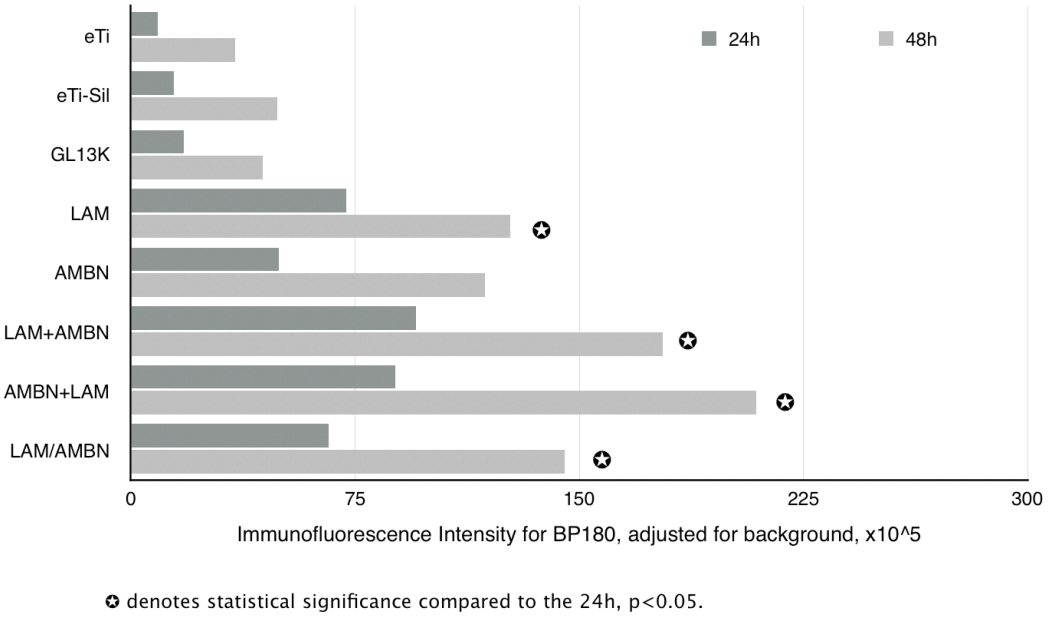

Figure 18. Hemidesmosome formation for the substrates over time.

Western Blot:

The results of the Western Blot at 48 hours confirmed the results of the Immunofluorescence for hemidesmosome formation on the Ti substrates (Figure 19). The mono-peptide groups, namely LAM and AMBN, as well as the combination groups, namely LAM+AMBN, AMBN+LAM and LAM/AMBN presented higher protein levels of collagen XVII (BP180), when compared to the control groups, namely: eTi, eTi-Sil and GL13K.

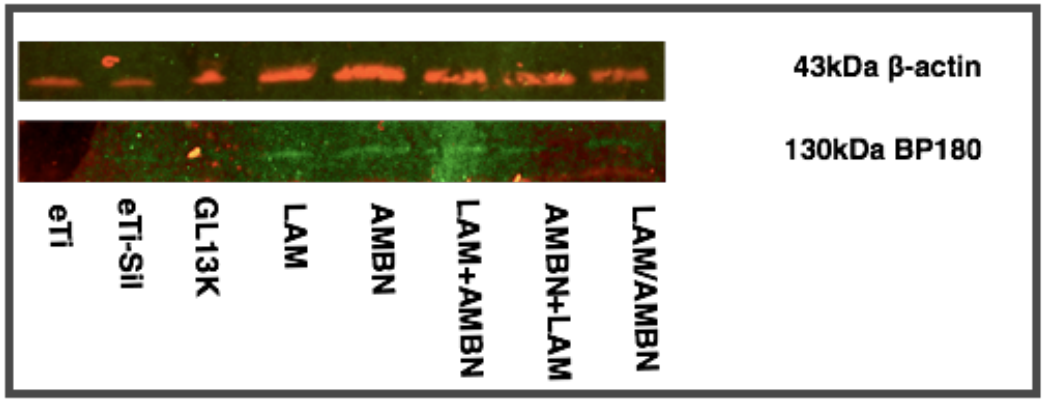

Figure 19. Western Blot at 48h for collagen XVII (BP180) and β-actin. (From left to right: ladder, eTi, eTi-Sil, GL13K, LAM, AMBN, LAM+AMBN, AMBN+LAM, LAM/AMBN) Red fluorescent labelling for β-actin and green fluorescent labelling for collagen XVII (BP180).

DISCUSSION

The aim of the present investigation was to evaluate the effect of a laminin derived (LAM), an ameloblastin derived (AMBN) peptide or combinations of both peptides on keratinocyte proliferation and hemidesmosome formation. In addition, the efficacy of immobilization of LAM, AMBN or combinations of both peptides and the mechanical and thermochemical stability of the produced substrates was assessed. The wettability of the produced substrates was assessed via contact angle goniometry (Figure 7). Control etched substrates (eTi) presented with low contact angles that increased (eTi-Sil) after the silanization process, due to the presence of the hydrophobic alkyl chains of the organosilanes. After immobilization of LAM, AMBN or combinations of both peptides, all coated surfaces presented with intermediate contact angle values, which were slightly higher than the control etched or silanized substrates, except when AMBN was immobilized alone (AMBN) or as the first peptide in sequential immobilization (AMBN+LAM). This finding is attributed to the pronounced polarity of the AMBN peptide, due to the higher hydrophilic/hydrophobic amino-acids ratio, relative to LAM. In addition, G13K substrates presented with significantly higher contact angles, when compared to the control (eTi, eTi-Sil) or the rest of the peptide-coated groups, as expected. Our group has significant experience with GL13K coated peptides and the response of the GL13K coated substrates confirm our previous results (*Chen 2014*). Thus, the included GL13K peptide group successfully served as a positive control in our experimental design.

Furthermore, subjecting the substrates to the mechanical and thermochemical challenges significantly altered the wettability properties of the peptide coated groups, as assessed by an increase in the contact angles for all peptide groups,

namely LAM, AMBN, LAM+AMBN, AMBN+LAM, LAM/AMBN. The changes in the surface wettability observed may be attributed either to the release of the peptides during the challenges or to the rearrangement and the possible conformational changes of the immobilized peptides.

In order to further verify the presence of the immobilized peptides on the substrates, XPS analysis was completed before and after the mechanical and thermochemical challenges (Figures 8, 9, 10). The increase in the nitrogen content for all groups subjected to peptide immobilization (GL13K, LAM, AMBN, LAM+AMBN, AMBN+LAM, LAM/AMBN) verified the presence of the peptides on the substrates. Furthermore, the increased nitrogen content for all peptide groups slightly decreased, but remained higher than the control groups (eTi, eTi-Sil) even after the mechanical and thermochemical challenges (Table 3). The nitrogen peak and the % atomic composition for nitrogen presented the lowest values for the AMBN group, relative to the rest of the peptide coated groups. However, they were higher than the control uncoated groups (eTi, eTi-Sil) and remained stable after the challenges. These findings are further confirmation of the successful immobilization of the peptides on the substrates and the appropriate stability of the immobilized peptides.

Additionally, qualitative analysis of the produced immobilized substrates included visualization of the peptides via immunofluorescence. Untreated eTi, or eTI-Sil surfaces, utilized as control, displayed no fluorescent signal. The fluorescence labelling further verified the presence of the peptides on the substrates (Figure 11), and in the case of the combination groups (LAM+AMBN, AMBN+LAM, LAM/AMBN), highlighted the simultaneous presence of both LAM and AMBN peptides, as assessed by the orange signal in the merged channel. Furthermore, the substrates were found to consist of homogeneously distributed LAM and AMBN peptides that

remained anchored on the substrates after the mechanical and thermochemical challenges.

Consequently, the results of the characterization for the produced substrates reveal that the LAM, AMBN or combinations of both peptides (LAM+AMBN, AMBN+LAM, LAM/AMBN) were successfully immobilized on the Ti substrates using covalent peptide bonding. Furthermore, after the mechanical and thermochemical challenges the substrates were found resistant to the complete removal of the peptides from the titanium substrates. As such, the changes observed in the water contact angles after the challenges may be attributed to a possible rearrangement of the immobilized peptides, rather than a release of the peptides.

Earlier attempts of physical absorption of organic molecules by immersion of the substrate in a solution of interest have been pursued. Major drawbacks of physical absorption of biomolecules are the lack of control for peptide density, lack of mechanical and physical chemical stability of the molecules on the coated surface and potential conformational changes of the directly adsorbed molecules, with respect to their natural active configuration (*Nazarpour 2014, Schliephake 2008*). Covalent bonding of the peptides, as utilized in the present investigation, leads to biomolecules' coating that is more robust and with notable resistance in disruption or detachment from the surface.

Regarding the effect of the produced substrates on keratinocytes, at 48h the mono-peptide experimental groups (LAM and AMBN) demonstrated superior OKF-6/TETR-2 proliferation, as compared to the control ($p<0.01$) or the combination groups (Figure 14). Our results agree with Oh et al. who described a significant role for the laminin 332 peptide (LAM) in the promotion of cell growth of keratinocytes and anti-apoptosis *(Oh 2009).* In contrast, Saito et al. concluded that ameloblastin suppresses epithelial proliferation and as such can prevent the epithelial down-growth or initiation

of periodontitis *(Saito 2014)*. The present investigation found that AMBN presented a significantly superior number of cells on the substrates at 48h, when compared to the controls (eTi, eTi-Sil, GL13K), similarly with LAM and with no statistically significant difference between the two groups. Furthermore, it becomes evident that the peptides' immobilization does not negatively affect the keratinocyte proliferation, since for all examined groups, except for the LAM+AMBN group, cell proliferation continues to increase over time (up to 48 hours) (Figure 15).

Regarding the formation of hemidesmosomes, immobilized substrates with combinations of both peptides -with sequential or simultaneous immobilization (LAM+AMBN, AMBN+LAM, LAM/AMBN), favored hemidesmosome formation on the Ti substrates at 48 hours, when compared with the untreated (eTi), silanized (eTi-Sil) or immobilization of an antimicrobial control peptide (GL13K) ($p<0.05$) (Figure 17).

The findings of this present investigation are in agreement with data from previous investigations regarding the role of laminin 332 in the promotion of hemidesmosome formation (*Tamura 1997, El-Grannam 1998, Werner 2009*). Previous investigations utilized either immersion of the substrate in a solution of the protein (*Tamura 1997, El-Grannam 1998*), incorporation in a scaffold of Type I collagen (*Damodaran 2013)* or incorporation of the peptide in a multilayered poly-electrolyte film (*Werner 2009*). Furthermore, the present investigation is the first to examine the effect of an ameloblastin derived peptide (AMBN) on keratinocytes' hemidesmosome formation. Several previous investigations up to date support that ameloblastin is being involved in processes other than amelogenesis, during tooth formation *(Spahr 2006, Nunez 2010, Hasegawa 2003)*, and the present investigation adds to the evidence that ameloblastin may hold a critical role in the attachment of the junctional epithelium around teeth and implants.

Finally, this investigation is the first to reveal that combinations of laminin 332 and ameloblastin derived peptides promote significantly higher formation of hemidesmosomes on the substrates at 24 and 48 hours, as assessed quantitatively via Immunofluorescence staining and qualitatively via Western Blot.

Interestingly, the combination groups namely: LAM+AMBN, AMBN+LAM and LAM/AMBN display a pronounced increase in cell numbers at early time points (1h, 24h), while the mono-peptide groups (LAM, AMBN) show the highest cell numbers at 48h (Figure 15). At the same time, the combination groups (LAM+AMBN, AMBN+LAM, LAM/AMBN) display higher hemidesmosome formation at 24 and 48h, when compared to the mono-peptide groups (LAM, AMBN) (Figure 18). Roshan et al. in 2016 demonstrated that keratinocytes possess two inter-changeable modes of proliferation, the balanced mode and the expanding mode, and suggested a model according to which keratinocytes switch from the expanding mode to the balanced mode when keratinocyte confluence is achieved. Upon that switch, keratinocytes differentiate. Similarly, when the confluence is disrupted, keratinocytes switch back to the expanding mode until the confluence is restored (*Roshan 2016).* In this context, in the present investigation the combination groups (LAM+AMBN, AMBN+LAM, LAM/AMBN) represent the expanding mode at early time points while switch to the balanced mode by 48h, reaching a critical confluence earlier than the rest of the examined groups (LAM, AMBN), thus allowing for hemidesmosome formation at earlier time points. This finding suggests that the combinations of both peptides enhance their properties by accelerating the processes of both keratinocyte proliferation and hemidesmosome formation.

A key finding of this study is the potential role of LAM, AMBN or their combinations to promote keratinocyte attachment around a titanium substrate may be translated clinically in the effort to reinforce the functional barrier against the microorganisms'

infiltration around dental implants and abutments with the prospect of preventing the development of peri-implant inflammation and peri-implantitis. The immobilization of the two above discussed peptides (LAM, AMBN) as a coating of a titanium substrate may provide the surrounding soft tissues with the stimuli that synergistically will induce healing and epithelial cell attachment on the titanium surface after implant placement. Our group has also developed methods to covalently immobilize various peptides on zirconia, which can be translated into an effort to functionalize implant abutments and other prosthetic components (*Fernandez-Garcia 2015*). For the present investigation, the combinations of both peptides may accelerate the switch of keratinocytes between the expanding mode to the balanced mode, contributing to the establishment of a stable per-mucosal seal at earlier time points after implant placement. In this context, the immobilization of the aforementioned peptides may prove useful in protecting the peri-implant tissues from peri-implantitis through the establishment of a stable per-mucosal seal.

CONCLUSIONS

1. The LAM, AMBN or combinations of both peptides were successfully immobilized on the Ti substrates.

2. The produced substrates presented mechanical and thermochemical stability, while the anchored peptides were homogenously distributed in both the monopeptide coatings as well as the combination coatings of LAM and AMBN.

3. The immobilization of the laminin 332 derived peptide (LAM) or the ameloblastin derived peptide (AMBN) significantly promotes keratinocyte proliferation at 48h.

4. The combinations of both peptides (LAM+AMBN, AMBN+LAM, LAM/AMBN) demonstrate higher hemidesmosome formation on the Ti substrates at 48h.

5. The combinations of both peptides (LAM+AMBN, AMBN+LAM, LAM/AMBN) accelerate the switch between the expanding mode and the balanced mode of keratinocytes.

6. LAM and AMBN peptide coatings are preferential candidates to establish a stable per-mucosal seal around dental implants.

BIBLIOGRAPHY

Atsuta I, Yamaza T, Yoshinari M, Goto T, Kido MA, Kagiya T, Mino S, Shimono M, Tanaka T. Ultrastructural localisation of laminin-5 (gamma2 chain) in the rat peri-implant oral mucosa around a titanium-dental implant by immuno-electron microscopy. Biomaterials. 2005; 26(32): 6280-7.

Aumailley M, Bruckner-Tuderman L, Carter WG, Deutzmann R, Edgar D, Ekblom P, Engel J, Engvall E, Hohenester E, Jones JC, Kleinman HK, Marinkovich MP, Martin GR, Mayer U, Meneguzzi G, Miner JH, Miyazaki K, Patarroyo M, Paulsson M, Quaranta V, Sanes JR, Sasaki T, Sekiguchi K, Sorokin LM, Talts JF, Tryggvason K, Uitto J, Virtanen I, von der Mark K, Wewer UM, Yamada Y, Yurchenco PD. A simplified laminin nomenclature. Matrix Biol. 2005; 24(5): 326-32.

Baker SE, Hopkinson SB, Fitchmun M, Andreason GL, Frasier F, Plopper G, Quaranta V, Jones JC. Laminin-5 and hemidesmosomes: role of the alpha 3 chain subunit in hemidesmosome stability and assembly. J Cell Sci. 1996; 109 (10): 2509-20.

Belkin AM, Stepp MA. Integrins as receptors for laminins. Microsc Res Techn 2000; 51(3): 280–301.

Berglundh T, Lindhe J, Ericsson I, Marinello CP, Liljenberg B, Thomsen P. The soft tissue barrier at implants and teeth. Clin Oral Implants Res. 1991; 2(2): 81-90.

Beyeler M, Schild C, Lutz R, Chiquet M, Trueb B. Identification of a fibronectin interaction site in the extracellular matrix protein ameloblastin. Exp Cell Res. 2010; 316(7): 1202-12.

Bosshardt DD, Lang NP. The junctional epithelium: from health to disease. J Dent Res 2005; 84(1): 9-20.

Burgeson RE, Chiquet M, Deutzmann R, Ekblom P, Engel J, Kleinman H, Martin GR, Meneguzzi G, Paulsson M, Sanes J et al. A new nomenclature for the laminins. Matrix Biol 1994; 14(3): 209–11.

Chen X, Sevilla P, Aparicio C. Surface biofunctionalization by covalent co-immobilization of oligopeptides. Colloids Surf B Biointerfaces. 2013 Jul 1; 107: 189-97.

Chen X, Hirt H, Li Y, Gorr S, Conrado A. Antimicrobial GL13K peptide coatings killed and ruptured the wall of streptococcus gordonii and prevented formation and growth of biofilms. PLoS ONE 9(11): e111579.

Colognato H, Yurchenco PD. Form and function: the laminin family of heterotrimers. Dev Dyn 2000; 218(2): 213–34.

Damodaran G, Tiong WH, Collighan R, Griffin M, Navsaria H, Pandit A. In vivo effects of tailored laminin-332 α3 conjugated scaffolds enhances wound healing: a histomorphometric analysis. J Biomed Mater Res A. 2013; 101(10): 2788-95.

Ebihara N, Mizushima H, Miyazaki K, Watanabe Y, Ikawa S, Nakayasu K, Kanai A. The functions of exogenous and endogenous laminin-5 on corneal epithelial cells. Exp Eye Res. 2000; 71(1): 69-79.

El-Ghannam A, Starr L, Jones J. Laminin-5 coating enhances epithelial cell attachment, spreading, and hemidesmosome assembly on Ti-6A1-4V implant material in vitro. J Biomed Mater Res. 1998; 41(1): 30-40.

Fernandez-Garcia E, Chen X, Gutierrez-Gonzalez CF, Fernandez A, Lopez-Esteban S, Aparicio C. Peptide-functionalized zirconia and new zirconia/titanium biocermets for dental applications. Journal of Dentistry 2015.

Fine JD, Bruckner-Tuderman L, Eady RA, Bauer EA, Bauer JW, Has C, Heagerty A, Hintner H, Hovnanian A, Jonkman MF, Leigh I, Marinkovich MP, Martinez AE, McGrath JA, Mellerio JE, Moss C, Murrell DF, Shimizu H, Uitto J, Woodley D, Zambruno G. Inherited epidermolysis bullosa: updated recommendations on diagnosis and classification. J Am Acad Dermatol 2014; 70: 1103-1126.

Fuchs E, Dowling J, Segre J, Lo SH, Yu QC. Integrators of epidermal growth and differentiation: distinct functions for beta 1 and beta 4 integrins. Curr Opin Genet Dev. 1997; 7(5): 672-82.

Fujii N, Kusakari H, Maeda T. A histological study on tissue responses to titanium implantation in rat maxilla: the process of epithelial regeneration and bone reaction. J Periodontol. 1998; 69(4): 485-495.

Fukushima Y, Ohnishi T, Arita N, Hayakawa T, Sekiguchi K. Integrin a3b1-mediated interaction with laminin-5 stimulates adhesion, migration and invasion of malignant glioma cells. Int J Cancer 1998; 76: 63–72.

Fukushima Y, Ohnishi T, Arita N, Hayakawa T, Sekiguchi K. Integrin a3b1- mediated interaction with laminin-5 stimulates adhesion, migration and invasion of malignant glioma cells. Int J Cancer 1998; 76(1): 63–72.

Hasegawa N, Kawaguchi H, Ogawa T, Uchida T, Kurihara H. Immunohistochemical characteristics of epithelial cell rests of Malassez during cementum repair. J Periodontal Res 2003; 38(1): 51–6.

Hieda Y, Nishizawa Y, Uematsu J, Owaribe K. Identification of a new hemidesmosomal protein, HD1: a major, high molecular mass component of isolated hemidesmosomes. J Cell Biol 1992; 116(6): 1497-1506.

Hirosaki T, Mizushima H, Tsubota Y, Moriyama K, Miyazaki K. Structural requirement of carboxyl-terminal globular domains of laminin alpha 3 chain for promotion of rapid cell adhesion and migration by laminin-5. J Biol Chem. 2000; 275(29): 22495-502.

Hormia M, Owaribe K, Virtanen I. The dento-epithelial junction: cell adhesion by type I hemidesmosomes in the absence of a true basal lamina. J Periodontol 2001; 72: 788-797.

Hormia M, Sahlberg C, Thesleff I, Airenne T. The epithelium-tooth interface--a basal lamina rich in laminin-5 and lacking other known laminin isoforms. J Dent Res 1998; 77(7): 1479-85.

Ikeda H, Yamaza T, Yoshinari M, Ohsaki Y, Ayukawa Y, Kido MA, Inoue T, Shimono M, Koyano K, Tanaka T. Ultrastructural and immunoelectron microscopic studies of the peri-implant epithelium-implant (Ti-6Al-4V) interface of rat maxilla. J Periodontol 2000; 71: 961–73.

Junker, R. Effects of implant surface coatings and composition on bone integration: a systematic review. Clin Oral Implants Res 2009; 20: 185-206.

Kim JM, Park WH, Min BM. The PPFLMLLKGSTR motif in globular domain 3 of the human laminin-5 alpha3 chain is crucial for integrin alpha3beta1 binding and cell adhesion. Exp Cell Res. 2005; 304(1): 317–27.

Kinumatsu T, Hashimoto S, Muramatsu T, Sasaki H, Jung HS, Yamada S, Shimono M. Involvement of laminin and integrins in adhesion and migration of junctional epithelium cells. J Periodontal Res. 2009; 44(1): 13-20.

Kogaya Y, Haruna S, Vojinovic J, Iwayama Y, Akisaka T. Histochemical localization at the electron microscopic level of sulfated glycosaminoglycans in the rat gingiva. J Periodontal Res 1989; 24: 199-206.

Krebsbach PH, Lee SK, Matsuki Y, Kozak CA, Yamada KM, Yamada Y. Full-length sequence, localization, and chromosomal mapping of ameloblastin. A novel tooth specific gene. J Biol Chem 1996; 271(8): 4431–5.

Lee SK, Krebsbach PH, Matsuki Y, Nanci A, Yamada KM, Yamada Y. Ameloblastin expression in rat incisors and human tooth germs. Int J Dev Biol 1996; 40(6): 1141–50.

Lindhe J. 2008. Clinical Periodontology and Implant Dentistry. 5th Edition. Volume 1, Oxford, Blackwell Munksgaard.

Listgarten MA. Electron microscopic features of the newly formed epithelial attachment after gingival surgery. A preliminary report. J Periodontal Res. 1967; 2(1): 46-52.

Min SK, Lee SC, Hong SD, Chung CP, Park WH, Min BM. The effect of a laminin-5-derived peptide coated onto chitin microfibers on re-epithelialization in early-stage wound healing. Biomaterials. 2010; 31(17): 4725-30.

Miner JH, Yurchenco PD. Laminin functions in tissue morphogenesis. Annu Rev Cell Dev Biol. 2004; 20: 255-84.

Mizushima H, Takamura H, Miyagi Y, Kikkawa Y, Yamanaka N, Yasumitsu H, Misugi K, Miyazaki K. Identification of integrin-dependent and -independent cell adhesion domains in COOH-terminal globular region of laminin-5 alpha 3 chain. Cell Growth Differ. 1997; 8(9): 979-87.

Mullen LM, Richards DW, Quaranta V. Evidence that laminin-5 is a component of the tooth surface internal basal lamina, supporting epithelial cell adhesion. J Periodontal Res. 1999; 34(1): 16-24.

Nazarpour S. 2014. Thin Films and Coatings in Biology. Edition: 1. Springer, Netherlands, pp. 105-143.

Nishio C, Wazen R, Kuroda S, Moffatt P, Nanci A. Disruption of periodontal integrity induces expression of apin by epithelial cell rests of Malassez. J Periodontal Res. 2010; 45(6): 709-13.

Nishiuchi R, Takagi J, Hayashi M, Ido H, Yagi Y, Sanzen N, Tsuji T, Yamada M, Sekiguchi K. Ligand-binding specificities of laminin-binding integrins: a comprehensive survey of laminin-integrin interactions using recombinant alpha3beta1, alpha6beta1, alpha7beta1 and alpha6beta4 integrins. Matrix Biol. 2006; 25(3): 189-97.

Nunez J, Sanz M, Hoz-Rodrıguez L, Zeichner-David M, Arzate H. Human cementoblasts express enamel-associated molecules in vitro and in vivo. J Periodontal Res 2010; 45(6): 809–14.

Oh JE, Jang DH, Kim H, Kang HK, Chung CP, Park WH, Min BM. alpha3beta1 integrin promotes cell survival via multiple interactions between 14-3-3 isoforms and proapoptotic proteins. Exp Cell Res. 2009; 315(18): 3187-200.

Oksonen J, Sorokin LM, Virtanen, Hormia M. The junctional epithelium around murine teeth differs from gingival epithelium in its basement membrane composition. J Dent Res. 2001; 80(12): 2093-7.

Owaribe K, Kantenbech J, Stumpp S, Magin TM, Krieg T, Diaz LA, Franke WW. The hemidesmosomal plaque. I. Characterisation of a major constituent protein as a differentiation marker for certain forms of epithelial. Differentiation 1990; 45:207-220.

Oyarzun-Droguett A. Ultracytochemical localization of basal lamina anionic sites in the rat epithelial attachment apparatus. J Periodontal Res 1992; 27: 256-263.

Ozawa T, Tsuruta D, Jones J, Ishii M, Ikeda K, Harada T, Aoyama Y, Kawada A, Kobayashi H. Dynamic relationship of focal contacts and hemidesmosome protein complexes in live cells. Journal of Investigative Dermatology 2000; 130: 1624-1635.

Palmquist, A. Titanium oral implants: surface characteristics, interface biology and clinical outcome. J R Soc Interface 2010; 7: S515-527.

Roshnan A, Murai K, Fowler J, Simons BD, Nikolaidou-Neokosmidou V, Jones PH. Human keratinocytes have two interconvertible modes of proliferation. Nat Cell Biol 2016; 18(2): 145-56.

Saito N, Ariyoshi W, Okinaga T, Kamegawa M, Matsukizono M, Akebiyama Y, Kitamura C, Nishihara T. Inhibitory effects of ameloblastin on epithelial cell proliferation. Arch Oral Biol. 2014; 59(8): 835-40.

Salonen J, Santti R. Ultrastructural and immunohistochemical similarities in the attachment of human oral epithelium to the tooth in vivo and to an inert substrate in an explant culture. J Periodontal Res. 1985; 20(2): 176-84.

Salonen J, Uitto VJ, Pan YM, Oda D. Proliferating oral epithelial cells in culture are capable of both extracellular and intracellular degradation of interstitial collagen. Matrix 1991; 11: 43-55.

Salonen JI, Kautsky MB, Dale BA. Changes in cell phenotype during regeneration of junctional epithelium of human gingiva in vitro. J Periodontal Res. 1989; 24(6): 370-7.

Sawada T, Yamamoto T, Yanagisawa T, Takuma S, Hasegawa H, Watanabe K. Electron-immunocytochemistry of laminin and type-IV collagen in the junctional epithelium of rat molar gingiva. J Periodontal Res 1990; 25: 372-376.

Sawada T, Yamazaki T, Shibayama K, Kumazawa Y, Ohshima M. Expression and localisation of laminin 5, laminin 10, type IV collagen, and amelotin in adult murine gingiva J Mol Histol. 2014; 45(3): 293-302.

Sawada T, Yamazaki T, Shibayama K, Yamaguchi Y, Ohshima M. Ultrastructural immunolocalization of laminin 332 (laminin 5) at dento-gingival interface in Macaca fuscata monkey. Med Mol Morphol. 2015; 48(2): 104-11.

Schaudinn C, Gorur A, Keller D, Sedghizadeh PP, Costerton JW. Periodontitis: An Archetypical Biofilm Disease. J Am Dent Assoc 2009; 140: 978-98.

Schliephake H, Scharnweber D. Chemical and biological functionalisation of titanium for dental implants, J. Mater. Chem. 2008; 18: 2404–2414.

Schroeder HE. 1977. Fine structure of the developing epithelial attachment of human teeth. Monographs in developmental biology. 2nd edition, Vol. 2. Wolsky A, Basel: Karger.

Shang M, Koshikawa N, Schenk S, Quaranta V. The LG3 module of laminin-5 harbors a binding site for integrin alpha3beta1 that promotes cell adhesion, spreading, and migration. J Biol Chem. 2001; 276(35): 33045-53.

Spahr A, Lyngstadaas SP, Slaby I, Pezeshki G. Ameloblastin expression during craniofacial bone formation in rats. Eur J Oral Sci 2006; 114(6): 504–11.

Streuli CH, Akhtar N. Signal co-operation between interns and other receptor systems. Biochem J 2009; 418: 491-506

Talts JF, Mann K, Yamada Y, Timpi R. Structural analysis and proteolytic processing of recombinant G domain of mouse laminin a2 chain. FEBS Lett. 1998; 426(1): 71–76.

Tamura RN, Oda D, Quaranta V, Plopper G, Lambert R, Glaser S, Jones JC. Coating of titanium alloy with soluble laminin-5 promotes cell attachment and hemidesmosome assembly in gingival epithelial cells: potential application to dental implants. J Periodontal Res. 1997; 32(3): 287-94.

Ten Cate AR. 1998. Development of the periodontium. Oral histology: Development, structure, and function. St. Louis: Mosby, pp. 236-252.

Ten Cate AR. The role of epithelium in the development, structure and function of the tissues of tooth support. Oral Dis. 1996; 2(1): 55-62.

Timpl R, Tisi D, Talts JF, Andac Z, Sasaki T, Hohenester E. Structure and function of laminin LG modules. Matrix Biol. 2000; 19: 309– 317.

Tsubota Y, Mizushima H, Hirosaki T, Higashi S, Yasumitsu H, Miyazaki K. Isolation and activity of proteolytic fragment of laminin-5 alpha3 chain. Biochem Biophys Res Commun. 2000; 278(3): 614-20.

Walco G, Castañón MJ, Wiche G. Molecular architecture and function of the hemidesmosome. Cell Tissue Res 2015; 360: 529-544.

Wazen RM, Moffatt P, Zalzal SF, Yamada Y, Nanci A. A mouse model expressing a truncated form of ameloblastin exhibits dental and junctional epithelium defects. Matrix Biol. 2009; 28(5): 292-303.

Werner S, Huck O, Frisch B, Vautier D, Elkaim R, Voegel JC, Brunel G, Tenenbaum H. The effect of microstructured surfaces and laminin-derived peptide coatings on soft tissue interactions with titanium dental implants. Biomaterials. 2009; 30(12): 2291-301.

Yamashita H, Shang M, Tripathi M, Jourquin J, Georgescu W, Liu S, Weidow B, Quaranta V. Epitope mapping of function-blocking monoclonal antibody CM6 suggests a “weak” integrin binding site on the Laminin-332 LG2 domain. J Cell Physiol. 2010; 223(3): 541–548.

Yurchenco PD. Basement membranes: cell scaffoldings and signaling platforms. Cold Spring Harb Perspect Biol. 2011; 3:a004911.

Zeichner-David M, Chen LS, Hsu Z, Reyna J, Caton J, Bringas P. Amelogenin and ameloblastin show growth-factor like activity in periodontal ligament cells. Eur J Oral Sci. 2006; 114 Suppl 1: 244-53; discussion 254-6, 381-2.

Zhang K, Kramer RH. Laminin 5 deposition promotes keratinocyte motility. Exp Cell Res. 1996; 227(2): 309-22.

Zhang Y, Zhang X, Lu X, Atsawasuwan P, Luan X. Ameloblastin regulates cell attachment and proliferation through RhoA and p27. Eur J Oral Sci. 2011;119 Suppl 1: 280-5.